PHYSICAL REVIEW D **71,** 054013 (2005)

Probing electroweak top quark couplings at hadron colliders

U. Baur*
Department of Physics, State University of New York, Buffalo, New York 14260, USA

A. Juste†
Fermi National Accelerator Laboratory, Batavia, Illinois 60510, USA

L. H. Orr‡ and D. Rainwater§
Department of Physics and Astronomy, University of Rochester, Rochester, New York 14627, USA
(Received 1 December 2004; published 11 March 2005)

We consider QCD $t\bar{t}\gamma$ and $t\bar{t}Z$ production at hadron colliders as a tool to measure the $tt\gamma$ and ttZ couplings. At the Tevatron it may be possible to perform a first, albeit not very precise, test of the $tt\gamma$ vector and axial vector couplings in $t\bar{t}\gamma$ production, provided that more than 5 fb^{-1} of integrated luminosity are accumulated. The $t\bar{t}Z$ cross section at the Tevatron is too small to be observable. At the CERN Large Hadron Collider (LHC) it will be possible to probe the $tt\gamma$ couplings at the few-percent level, which approaches the precision which one hopes to achieve with a next-generation e^+e^- linear collider. The LHC's capability of associated QCD $t\bar{t}V$ ($V = \gamma, Z$) production has the added advantage that the $tt\gamma$ and ttZ couplings are not entangled. For an integrated luminosity of 300 fb^{-1}, the ttZ vector (axial vector) coupling can be determined with an uncertainty of $45 - 85\%$ ($15 - 20\%$), whereas the dimension-five dipole form factors can be measured with a precision of $50 - 55\%$. The achievable limits improve typically by a factor of $2 - 3$ for the luminosity-upgraded (3 ab^{-1}) LHC.

DOI: 10.1103/PhysRevD.71.054013 PACS numbers: 14.65.Ha, 13.85.Qk

I. INTRODUCTION

Although the top quark was discovered almost ten years ago [1,2], many of its properties are still only poorly known [3]. In particular, the couplings of the top quark to the electroweak (EW) gauge bosons have not yet been directly measured. The large top quark mass [4] suggests that it may play a special role in EW symmetry breaking (EWSB). New physics connected with EWSB may thus be found first in top quark precision observables. A possible signal for new physics are deviations of the $tt\gamma$, ttZ and tbW couplings from the values predicted by the Standard Model (SM). For example, in technicolor and other models with a strongly coupled Higgs sector, anomalous top quark couplings may be induced at the $5 - 10\%$ level [5].

Current data provide only weak constraints on the couplings of the top quark with the EW gauge bosons, except for the ttZ vector and axial vector couplings which are rather tightly but indirectly constrained by LEP data (see Sec. II C); and the right-handed tbW coupling, which is severely bound by the observed $b \to s\gamma$ rate [6]. In future, the tbW vertex can be probed in top quark decays to Wb [7–10], single-top quark production at hadron colliders [11–14], $e\gamma$ collisions [15], and top pair production at an e^+e^- linear collider [16–18]. The $tt\gamma$ and ttZ couplings can also be tested in $e^+e^- \to t\bar{t}$ [17–23], and in $t\bar{t}V$ ($V = \gamma, Z$) production at hadron colliders [24,25]. Finally, the process $\gamma\gamma \to t\bar{t}$ is also sensitive to $tt\gamma$ couplings [26,27].

At an e^+e^- linear collider with $\sqrt{s} = 500$ GeV and an integrated luminosity of $100 - 200$ fb^{-1} one can hope to measure the ttV couplings in top pair production with a few-percent precision [20]. However, the process $e^+e^- \to \gamma^*/Z \to t\bar{t}$ is sensitive to both $tt\gamma$ and ttZ couplings and significant cancellations between the various couplings can occur. At hadron colliders, $t\bar{t}$ production is so dominated by the QCD processes $q\bar{q} \to g^* \to t\bar{t}$ and $gg \to t\bar{t}$ that a measurement of the $tt\gamma$ and ttZ couplings via $q\bar{q} \to \gamma^*/Z^* \to t\bar{t}$ is hopeless. Instead, the ttV couplings can be measured in QCD $t\bar{t}\gamma$ production, radiative top quark decays in $t\bar{t}$ events ($t\bar{t} \to \gamma W^+W^-b\bar{b}$), and QCD $t\bar{t}Z$ production. $t\bar{t}\gamma$ production and radiative top quark decays are sensitive only to the $tt\gamma$ couplings, whereas $t\bar{t}Z$ production gives information only on the structure of the ttZ vertex. This obviates having to disentangle potential cancellations between the different couplings. In these three processes one can also hope to separate the dimension-four and -five couplings which appear in the effective Lagrangian describing the ttV interactions. Helicity amplitudes of an operator with dimension n in general grow with energy, E, proportional to E^{n-4}. As a result, the shape of the photon or Z boson transverse momentum distribution differs considerably for couplings of different dimensionality.

In this paper we consider $t\bar{t}\gamma$ production (including radiative top quark decays in $t\bar{t}$ events), and $t\bar{t}Z$ production, at the Tevatron and LHC as a tool to measure the ttV couplings. We first review the couplings definitions, then discuss existing bounds on them, as well as constraints

*baur@ubhex.physics.buffalo.edu
†juste@fnal.gov
‡orr@pas.rochester.edu
§rain@pas.rochester.edu

from S-matrix unitarity (Sec. II). In Secs. III and IV we present detailed analyses of $t\bar{t}\gamma$ and $t\bar{t}Z$ production, including all relevant backgrounds. We derive sensitivity bounds in Sec. V, where we also present a detailed comparison with the limits anticipated at a future e^+e^- linear collider. We summarize in Sec. VI.

II. GENERAL ttV COUPLINGS

A. Definition

The most general Lorentz-invariant vertex function describing the interaction of a neutral vector boson V with two top quarks can be written in terms of ten form factors [28], which are functions of the kinematic invariants. In the low energy limit, these correspond to couplings which multiply dimension-four or -five operators in an effective Lagrangian, and may be complex. If V is on-shell, or if V couples to effectively massless fermions, the number of independent form factors is reduced to eight. If, in addition, both top quarks are on-shell, the number is further reduced to four. In this case, the ttV vertex can be written in the form

$$\Gamma_\mu^{ttV}(k^2, q, \bar{q}) = -ie\{\gamma_\mu[F_{1V}^V(k^2) + \gamma_5 F_{1A}^V(k^2)] + \frac{\sigma_{\mu\nu}}{2m_t}(q+\bar{q})^\nu[iF_{2V}^V(k^2) + \gamma_5 F_{2A}^V(k^2)]\}, \quad (1)$$

where e is the proton charge, m_t is the top quark mass, $q(\bar{q})$ is the outgoing top (antitop) quark four-momentum, and $k^2 = (q+\bar{q})^2$. The terms $F_{1V}^V(0)$ and $F_{1A}^V(0)$ in the low energy limit are the ttV vector and axial vector form factors. The coefficients $F_{2V}^\gamma(0)$ and $F_{2A}^\gamma(0)$ are related to the magnetic and (CP-violating) electric dipole form factors, g_t and d_t^γ accordingly:

$$F_{2V}^\gamma(0) = Q_t\frac{g_t - 2}{2}, \quad (2)$$

$$F_{2A}^\gamma(0) = \frac{2m_t}{e}d_t^\gamma, \quad (3)$$

where $Q_t = 2/3$ is the top quark electric charge. Similar relations hold for $F_{2V}^Z(0)$, $F_{2A}^Z(0)$, and the weak magnetic and weak electric dipole moments, g_t^Z and d_t^Z. At tree level in the SM,

$$\begin{aligned} F_{1V}^{\gamma,SM} &= -\frac{2}{3}, \qquad F_{1A}^{\gamma,SM} = 0, \\ F_{1V}^{Z,SM} &= -\frac{1}{4\sin\theta_W\cos\theta_W}\left(1 - \frac{8}{3}\sin^2\theta_W\right), \\ F_{1A}^{Z,SM} &= \frac{1}{4\sin\theta_W\cos\theta_W}, \qquad F_{2V}^{\gamma,SM} = F_{2V}^{Z,SM} = 0, \\ F_{2A}^{\gamma,SM} &= F_{2A}^{Z,SM} = 0, \end{aligned} \quad (4)$$

where θ_W is the weak mixing angle. The one-loop corrections to $F_{1V,A}^\gamma$ vanish for on-shell photons [29]. The numerically most important radiative corrections to the ttZ vector and axial vector couplings can be taken into account by replacing the factor $(1 - 8\sin^2\theta_W/3)$ in $F_{1V}^{Z,SM}$ by $(1 - 8\sin^2\theta_{eff}^t/3)$, where $\sin^2\theta_{eff}^t$ is the effective mixing angle, and by expressing the remaining factors of $\sin\theta_W$ and $\cos\theta_W$ in $F_{1V,A}^{Z,SM}$ in terms of the physical W and Z masses. Numerically, the one-loop corrections to $F_{1V,A}^V$ are typically of $\mathcal{O}(10^{-3} - 10^{-2})$ [29]. The magnetic and weak magnetic dipole form factors F_{2V}^V receive contributions of the same magnitude [30] at the one-loop level in the SM. However, there is no such contribution to the electric and weak electric dipole form factors, F_{2A}^V [28].

In $t\bar{t}V$ production, one of the top quarks coupling to V is off-shell. The most general vertex function relevant for $t\bar{t}V$ production thus contains additional couplings, not included in Eq. (1). These additional couplings are irrelevant in $e^+e^- \to t\bar{t}$, where both top quarks are on-shell. Since most of the existing literature does not discuss them, we ignore these additional couplings in the following.

In $e^+e^- \to t\bar{t}$ one often uses the following parametrization for the ttV vertex:

$$\Gamma_\mu^{ttV}(k^2, q, \bar{q}) = ie\left\{\gamma_\mu[\tilde{F}_{1V}^V(k^2) + \gamma_5\tilde{F}_{1A}^V(k^2)] + \frac{(q-\bar{q})_\mu}{2m_t}[\tilde{F}_{2V}^V(k^2) + \gamma_5\tilde{F}_{2A}^V(k^2)]\right\}. \quad (5)$$

Using the Gordon decomposition, it is easy to show that Eqs. (1) and (5) are equivalent and that the form factors $\tilde{F}_{iV,A}^V$ and $F_{iV,A}^V$ ($i = 1, 2$) are related by

$$\tilde{F}_{1V}^V = -(F_{1V}^V + F_{2V}^V), \quad (6)$$

$$\tilde{F}_{2V}^V = F_{2V}^V, \quad (7)$$

$$\tilde{F}_{1A}^V = -F_{1A}^V, \quad (8)$$

$$\tilde{F}_{2A}^V = -iF_{2A}^V. \quad (9)$$

It should be noted that the Gordon decomposition holds only if both top quarks are on-shell. Only in this case are the vertex functions of Eqs. (1) and (5) equivalent. We found that for our processes, $t\bar{t}V$ associated production, using the Gordon decomposition results in gross Lorentz violations of the matrix elements. We therefore base our analysis on the form factors in Eq. (1) and use Eqs. (6)–(9) only in Sec. V to compare the limits we obtain for $F_{iV,A}^V$ at the Tevatron and LHC with those listed in the literature for $\tilde{F}_{iV,A}^V$.

B. Unitarity Constraints

The parton-level production cross sections of processes such as $t\bar{t} \to VV$ or $t\bar{t} \to W^+W^-$ with non-SM ttV cou-

plings manifestly grow with the parton center-of-mass energy $\sqrt{\hat{s}}$. S-matrix unitarity restricts the ttV couplings uniquely to their SM values at asymptotically high energies [31]. This requires that the couplings $F^V_{iV,A}$ $(i = 1, 2)$ possess a momentum dependence which ensures that any deviations of the $F^V_{iV,A}(\hat{s})$ from their SM values vanish for $\hat{s} \gg m_t^2$. The precise $\hat{s}$-dependence of the couplings is, of course, unknown. The simplest possible ansatz is to assume a constant anomalous coupling for $\sqrt{\hat{s}} < \Lambda$ which abruptly drops to zero at $\sqrt{\hat{s}} = \Lambda$ (step-function) where the scale Λ is related to the scale of the new physics generating the anomalous couplings. This ansatz is generally used when calculating the contributions of nonstandard couplings to loop observables (see Sec. II C). Here, in order to explore how S-matrix unitarity restricts the anomalous ttV couplings, we use instead a dipole form factor, similar to the well-known nucleon form factor,

$$\Delta F^V_{iV,A}(k^2) = \frac{\Delta F^V_{iV,A}(0)}{(1 + k^2/\Lambda^2_{FF})^2} \quad (i = 1, 2), \tag{10}$$

where

$$\Delta F^V_{iV,A}(k^2) = F^V_{iV,A}(k^2) - F^{V,SM}_{iV,A}, \tag{11}$$

and Λ_{FF} is the form factor scale which is analogous to the scale Λ discussed above.

The values $\Delta F^V_{iV,A}(0)$ are constrained by partial wave unitarity of the amplitudes $t\bar{t} \to t\bar{t}$, $t\bar{t} \to W^+W^-$, $t\bar{t} \to VV$ and $t\bar{t} \to ZH$ (where H is the SM Higgs field) at arbitrary center-of-mass energies. The most stringent bounds are obtained from W^+W^- production in t–$\bar{t}$ annihilation. We find

$$|\Delta F^\gamma_{1V,A}(0)| \leq \frac{96\pi}{\sqrt{6}G_F} \frac{1}{\sin^2\theta_W} \frac{1}{\Lambda^2_{FF}} \approx \left(\frac{6.78\ \text{TeV}}{\Lambda_{FF}}\right)^2, \tag{12}$$

$$|\Delta F^Z_{1V,A}(0)| \leq \frac{96\pi}{\sqrt{6}G_F} \frac{1}{\sin\theta_W \cos\theta_W} \frac{1}{\Lambda^2_{FF}} \approx \left(\frac{5.01\ \text{TeV}}{\Lambda_{FF}}\right)^2, \tag{13}$$

$$|\Delta F^\gamma_{2V,A}(0)| \leq \frac{128\sqrt{2}\pi}{\sin^2\theta_W} \frac{m_t}{G_F} \frac{1}{\Lambda^3_{FF}} \approx \left(\frac{3.35\ \text{TeV}}{\Lambda_{FF}}\right)^3, \tag{14}$$

$$|\Delta F^Z_{2V,A}(0)| \leq \frac{128\sqrt{2}\pi}{\sin\theta_W \cos\theta_W} \frac{m_t}{G_F} \frac{1}{\Lambda^3_{FF}} \approx \left(\frac{2.75\ \text{TeV}}{\Lambda_{FF}}\right)^3, \tag{15}$$

where G_F is the Fermi constant and θ_W is the weak mixing angle. We use a top quark mass of 178 GeV [4] in Eqs. (12)–(15). Our results for $\Delta F^Z_{1V,A}(0)$ are consistent with those obtained in Ref. [32]. For a step-function form factor, the bounds on $\Delta F^Z_{1V,A}(0)$ $(\Delta F^Z_{2V,A}(0))$ in Equations (12) and (13) (Eqs. (14) and (15)) have to be divided by a factor four (16).

C. Present Experimental Limits

Although there are no current direct limits, precision measurements at the Z pole and the measured $b \to s\gamma$ branching ratio (BR) provide indirect limits on the ttV couplings. Nonstandard ttZ couplings and the $tt\gamma$ dipole form factors, $F^\gamma_{2V,A}$, contribute at one-loop to the ϵ parameters of Ref. [33]. The $b \to s\gamma$ BR gives additional information on the $F^\gamma_{2V,A}$ couplings. Nonstandard ttV coupling contributions to the ϵ parameters are divergent unless the couplings' momentum dependence is properly taken into account. As discussed in Sec. II B, one usually regularizes the divergent integrals by assuming the form factors to be of step-function form ($\theta(x)$ is the step-function):

$$\Delta F^V_{iV,A}(k^2) = \Delta F^V_{iV,A}(0)\theta(\Lambda^2 - k^2). \tag{16}$$

Extracting information on anomalous couplings from loop observables assumes that no other sources of new physics contribute to these observables.

Nonstandard ttZ vector and axial vector couplings, $\Delta F^Z_{1V,A}$, are mostly constrained by the parameters ϵ_1 and ϵ_b, which are closely related to the ρ parameter and the $Z \to b\bar{b}$ decay width. The terms proportional to $\Delta F^Z_{1V,A}$ which contribute to ϵ_2 and ϵ_3 are suppressed by a factor m_W^2/m_t^2 (where m_W is the mass of the W boson) relative to those which appear in ϵ_1 and ϵ_b. Using the expressions given in Ref. [6] combined with the most recent experimental results [34] and SM predictions [35] for the ϵ parameters, and assuming that the couplings $\Delta F^Z_{1V,A}$ are real, we obtain

$$-0.044 \leq -\Delta F^Z_{1A}(0)[1 + 0.842\Delta F^Z_{1A}(0)]\log\left(\frac{\Lambda^2}{m_t^2}\right) \leq 0.065, \tag{17}$$

$$-0.029 \leq -[\Delta F^Z_{1A}(0) - \frac{3}{5}\Delta F^Z_{1V}(0)]\log\left(\frac{\Lambda^2}{m_t^2}\right) \leq 0.143. \tag{18}$$

For $\Lambda = \mathcal{O}(1\ \text{TeV})$, Eqs. (17) and (18) constrain $|\Delta F^Z_{1V,A}(0)|$ to be less than a few percent.

The effect of the magnetic dipole moment couplings F^V_{2V} on the ϵ parameters was analyzed in Ref. [36]. It turns out that F^V_{2V} affects only ϵ_2 and ϵ_3 and that these parameters constrain only a combination of F^γ_{2V} and F^Z_{2V}. From the most recent experimental results and theoretical predictions for these parameters, one obtains:

$$-0.92 \leq -[F^\gamma_{2V}(0) + 1.83F^Z_{2V}(0)]\log\left(\frac{\Lambda^2}{m_t^2}\right) \leq 0, \tag{19}$$

$$-1.08 \leq -[F^\gamma_{2V}(0) + 1.83F^Z_{2V}(0)]\log\left(\frac{\Lambda^2}{m_t^2}\right) \leq 1.92, \tag{20}$$

where again we have assumed real F_{2V}^V. If only one of the couplings is allowed to deviate from its SM value, Eqs. (19) and (20) yield $|F_{2V}^\gamma(0)| \lesssim 0.3$ and $|F_{2V}^Z(0)| \lesssim 0.2$ for $\Lambda = 1$ TeV. The effect of the electric dipole moment couplings F_{2A}^V on the ϵ parameters has not been studied so far.

Bounds on $F_{2V,A}^\gamma$ from $b \to s\gamma$ data can easily be estimated from Refs. [6,37]. The latest CLEO and BELLE measurements of the $b \to s\gamma$ BR give $BR(b \to s\gamma) = (3.3 \pm 0.4) \cdot 10^{-4}$ [38]. The SM predicts $BR(b \to s\gamma) = (3.4 \pm 0.5 \pm 0.4) \cdot 10^{-4}$ [39], where the first error is an estimate of the perturbative uncertainties, and the second reflects uncertainties in the input parameters. Adding the experimental and theoretical uncertainties in quadrature, we find:

$$-0.39 \le 1.94\mathrm{Re}[F_{2V}^\gamma(0)] + 0.68\mathrm{Im}[F_{2A}^\gamma(0)] + 0.45|F_{2V}^\gamma(0)|^2 + 0.056|F_{2A}^\gamma(0)|^2 \le 1.11. \quad (21)$$

Assuming that F_{2V}^γ and F_{2A}^γ are real couplings, and varying only one coupling at a time, one finds that $-0.2 \le F_{2V}^\gamma(0) \le 0.5$[1] and $|F_{2A}^\gamma(0)| \le 4.5$.

The $tt\gamma$ vector and axial vector couplings are not constrained by any current data.

III. $t\bar{t}\gamma$ PRODUCTION

For $t\bar{t}\gamma$ production, as well as the $t\bar{t}Z$ process considered in the next section, we assume the Tevatron (LHC) to be operating at $\sqrt{s} = 2.0(14)$ TeV.

A. Signal

The process $p\bar{p}^{(-)} \to t\bar{t}\gamma$ followed by $t \to Wb$ leads either to a $\gamma\ell\nu_\ell\ell'\nu_{\ell'}b\bar{b}$ final state if both W bosons decay leptonically, to a $\gamma\ell\nu_\ell b\bar{b}jj$ final state if one W decays leptonically and the other decays hadronically, or to a $\gamma b\bar{b} + 4j$ final state if both W bosons decay hadronically. The $\gamma b\bar{b} + 4j$ final state has the largest BR. However, it is plagued by a large QCD background, so we ignore it. The dilepton final state, although less contaminated by background, has a BR about a factor six smaller than that of the so-called lepton+jets mode. In the following, we therefore concentrate on this last process:

$$p\bar{p}^{(-)} \to \gamma\ell\nu_\ell b\bar{b}jj \quad (22)$$

with $\ell = e, \mu$ (τ leptons are ignored). We assume that both b quarks are tagged with a combined efficiency of $\epsilon_b^2 = 25\%$ ($\epsilon_b^2 = 40\%$) at the Tevatron (LHC), unless explicitly stated otherwise.

We perform our calculation for general $tt\gamma$ couplings of the form of Eq. (1). As we shall see, at both the Tevatron and the LHC, photon transverse momenta of at most a few hundred GeV are accessible. The scale of new physics responsible for anomalous $tt\gamma$ couplings is expected to be of $\mathcal{O}(1\ \mathrm{TeV})$ or higher. Form factor effects will thus be small and are therefore neglected in the following. We also assume that all $tt\gamma$ couplings are real. We otherwise assume the SM to be valid. In particular, we assume that the $bb\gamma$ coupling is that of the SM. Our analysis for F_{1V}^γ thus differs from that of Ref. [25] for the top quark electric charge (Q_t) measurement. That study assumed that Q_t is related to the b quark charge, Q_b, and W boson charge, $Q_W = \pm 1$, by $Q_t = Q_b + Q_W$.

Our calculation includes top quark and W decays with full spin correlations and finite width effects. All resonant Feynman diagrams contributing to the lepton+jets final state are included, i.e., besides $t\bar{t}\gamma$ production, we automatically take into account top quark pair production where one of the top quarks decays radiatively, $t \to Wb\gamma$. Subsequently, we will refer to this process simply as "$t\bar{t}\gamma$ production" and it is implied that it automatically includes any contribution from $t\bar{t}$ production where one of the top quarks undergoes radiative decay. To ensure gauge invariance of the SM cross section, we use the so-called overall-factor scheme of Ref. [40], as implemented for $t\bar{t}V$ production in Ref. [41].

All signal and background cross sections in this paper are computed using CTEQ6L1 [42] parton distribution functions with the strong coupling constant evaluated at leading order and $\alpha_s(m_Z^2) = 0.130$, where m_Z is the Z-boson mass. The top quark mass is assumed to be $m_t = 178$ GeV [4]. All signal cross sections in this paper are calculated for factorization and renormalization scales equal to m_t.

The acceptance cuts for $\gamma\ell\nu_\ell b\bar{b}jj$ events at the Tevatron (LHC) are

$$\not{p}_T > 20\ \mathrm{GeV}, \quad p_T(b) > 15(20)\ \mathrm{GeV}, \quad |\eta(b)| < 2.0(2.5), \quad \Delta R(b,b) > 0.4, \quad p_T(j) > 20\ \mathrm{GeV}, \quad |\eta(j)| < 2.5, \quad \Delta R(j,j) > 0.4, \quad \Delta R(j,b) > 0.4, \quad p_T(\gamma) > 10(30)\ \mathrm{GeV}, \quad |\eta(\gamma)| < 2.5, \quad \Delta R(\gamma,j) > 0.4, \quad \Delta R(\gamma,b) > 1.0, \quad p_T(\ell) > 15\ \mathrm{GeV}, \quad |\eta(\ell)| < 2.5, \quad \Delta R(\ell,\gamma) > 0.4, \quad \Delta R(\ell,j) > 0.4, \quad \Delta R(\ell,b) > 0.4, \quad (23)$$

where $\Delta R = [(\Delta\Phi)^2 + (\Delta\eta)^2]^{1/2}$ is the separation in pseudorapidity – azimuth space and $\not{p}_T$ is the missing transverse momentum originating from the neutrino which escapes undetected. We include minimal detector effects via Gaussian smearing of parton momenta according to CDF [43] and CMS [44] expectations, and take into account the b jet energy loss via a parameterized function.

[1] A second solution, $-5.9 \le F_{2V}^\gamma(0) \le -4.1$ is clearly inconsistent with LEP data (see Eqs. (19) and (20)).

Since we are interested in photon emission from top quarks, we would like to suppress radiation from W decay products, as well as emission from b quarks and from initial-state quarks. The large $\Delta R(\gamma, b)$ cut in Eq. (23) reduces photon radiation from the b quarks. Photon emission from W decay products can essentially be eliminated by requiring that

$$m(jj\gamma) > 90 \text{ GeV} \quad \text{and} \quad m_T(\ell\gamma; \not{p}_T) > 90 \text{ GeV}, \quad (24)$$

where $m(jj\gamma)$ is the invariant mass of the $jj\gamma$ system. The variable $m_T(\ell\gamma; \not{p}_T)$ is the $\ell\gamma\not{p}_T$ cluster transverse mass, given by

$$m_T^2(\ell\gamma; \not{p}_T) = (\sqrt{p_T^2(\ell\gamma) + m^2(\ell\gamma)} + \not{p}_T)^2 - [\vec{p}_T(\ell\gamma) + \vec{\not{p}}_T]^2, \quad (25)$$

where $p_T(\ell\gamma)$ and $m(\ell\gamma)$ are the transverse momentum and invariant mass of the $\ell\gamma$ system, respectively. The $\ell\gamma\not{p}_T$ cluster transverse mass peaks sharply at m_W. It is difficult to suppress radiation from the initial-state quarks without simultaneously reducing the signal cross section by an equal amount. Fortunately this is not a problem at the LHC, where gluon fusion dominates.

In addition to the cuts listed in Eqs. (23) and (24), we require that the event is consistent either with $t\bar{t}\gamma$ production, or with $t\bar{t}$ production with radiative top decay. This will reduce the singly-resonant and nonresonant backgrounds, and is accomplished by selecting events which satisfy either

$$m_T(b_{1,2}\ell; \not{p}_T) < m_t + 20 \text{ GeV} \quad \text{and} \quad m_t - 20 \text{ GeV} < m(b_{2,1}jj) < m_t + 20 \text{ GeV}, \quad (26)$$

$$m_T(b_{1,2}\ell\gamma; \not{p}_T) < m_t + 20 \text{ GeV} \quad \text{and} \quad m_t - 20 \text{ GeV} < m(b_{2,1}jj) < m_t + 20 \text{ GeV}, \quad (27)$$

or

$$m_T(b_{1,2}\ell; \not{p}_T) < m_t + 20 \text{ GeV} \quad \text{and} \quad m_t - 20 \text{ GeV} < m(b_{2,1}jj\gamma) < m_t + 20 \text{ GeV}. \quad (28)$$

Here, $b_1, b_2 = b, \bar{b}$, and $b_1 \neq b_2$.

Imposing the cuts listed in Eqs. (23)–(28), and before taking into account particle identification efficiencies, we obtain a cross section of about 5 fb (82 fb) at the Tevatron (LHC). The total integrated luminosity one hopes to achieve at the Tevatron in Run II is between 4 and 8 fb^{-1}. While this will not be sufficient for a precision measurement of the $tt\gamma$ couplings, it may offer a chance for a first test of these couplings. At the LHC, with 300 fb^{-1}, one expects several thousand signal events which should make it possible to precisely determine the $tt\gamma$ couplings if the background can be controlled.

B. Background Processes

The most important irreducible background processes that remain after imposing the cuts described in Sec. III A, are $t(\to b\ell^+\nu)\bar{b}\gamma jj$, $\bar{t}(\to \bar{b}\ell^-\bar{\nu})b\gamma jj$, $t(\to bjj)\bar{b}\ell^-\bar{\nu}\gamma$ and $\bar{t}(\to \bar{b}jj)b\ell^+\nu\gamma$ production, and the nonresonant process $p^{(-)}p \to W(\to \ell\nu)\gamma b\bar{b}jj$. The single-top processes will be collectively denoted as "$(t\bar{b}\gamma + \bar{t}b\gamma) + X$ production" in the following. We calculate the irreducible background processes at leading order in QCD including the full set of contributing Feynman diagrams using MADEVENT [45]. $W(\to \ell\nu\gamma)b\bar{b}jj$ production, as well as $t\bar{b}jj$, $\bar{t}bjj$, $t\bar{b}\ell^-\bar{\nu}$ and $\bar{t}b\ell^+\nu$ production where the top quark decays radiatively, are strongly suppressed by the cuts of Eqs. (24)–(28) and therefore not considered.

There are also several reducible backgrounds resulting from light jets faking either b jets or photons, or from Z bosons where one of the leptons in $Z \to \ell^+\ell^-$ is lost and fakes missing transverse momentum. To estimate these backgrounds we assume the probability of a light jet to be misidentified as a b jet to be [46,47]

$$P_{j\to b} = 1/100 \quad (1/140) \quad (29)$$

at the Tevatron (LHC). For the probability of a jet to fake a photon, $P_{j\to\gamma}$, at the Tevatron we use the result obtained by CDF for 10 GeV $\leq p_T(\gamma) \leq$ 25 GeV in the measurement of the $W\gamma$ and $Z\gamma$ cross sections [48], and conservatively assume that $P_{j\to\gamma}$ is constant for $p_T(\gamma) \geq 25$ GeV:

$$P_{j\to\gamma} = \begin{cases} a \cdot e^{-b\cdot p_T(\gamma)} & \text{for} \quad 10 \text{ GeV} \leq \mathrm{p_T}(\gamma) \leq 25 \text{ GeV}, \\ 7 \cdot 10^{-4} & \text{for} \quad p_T(\gamma) \geq 25 \text{ GeV}, \end{cases} \quad (30)$$

with $a = 0.0079$ and $b = 0.097$ GeV^{-1}. The DØ Collaboration obtained a similar result [49]. Expectations for the probability to misidentify a light jet as a photon at the LHC vary between $P_{j\to\gamma}^{\text{lo}} = 1/2500$ and $P_{j\to\gamma}^{\text{hi}} = 1/1600$ [44,50–52]. In the following we take the conservative route and use the more pessimistic estimate $P_{j\to\gamma} = 1/1600$ for all numerical studies at LHC.

The potentially most dangerous reducible background is $t\bar{t}j$ production where one of the jets in the final state fakes a photon. We calculate this using exact $W^+W^-b\bar{b}j$ matrix elements, including spin correlations for the W decays. However, gluon radiation from the W decay products is not included. For the cuts used here, Eqs. (23)–(28), this should be an excellent approximation to the full process $p^{(-)}p \to \ell\nu b\bar{b} + 3$ jets.

In Fig. 1 we show the photon transverse momentum distributions of the $t\bar{t}\gamma$ signal (solid curve), the $t\bar{t}j$ background (dotted line), the background from single-top production processes (dashed line), and the $W\gamma b\bar{b}jj$ background (histogram). There are several thousand

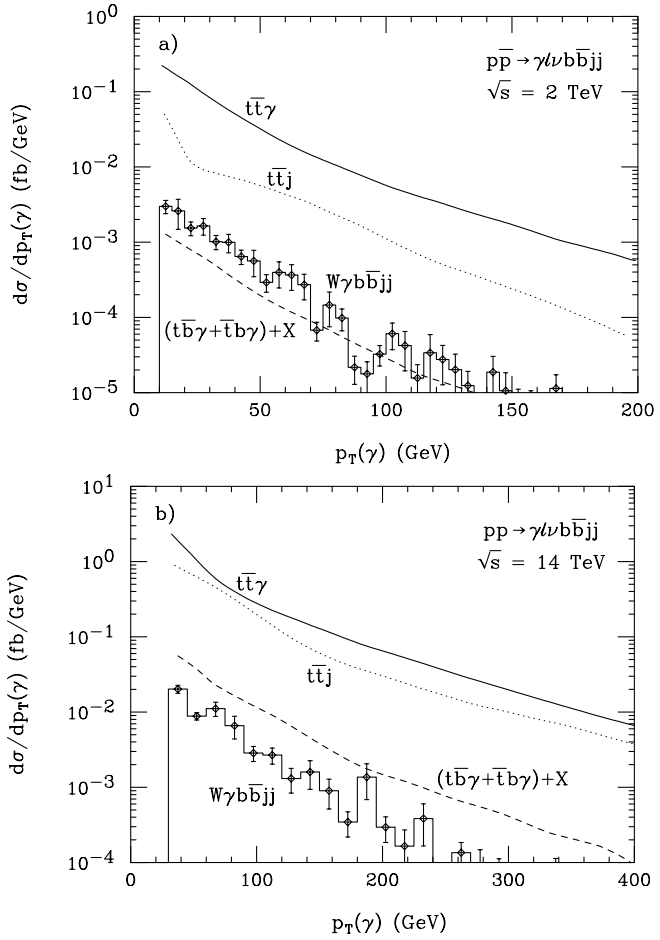

FIG. 1. The differential cross sections as a function of the photon transverse momentum for $\gamma\ell\nu_\ell b\bar{b}jj$ production at (a) Tevatron Run II and (b) LHC. Shown are the SM predictions for $t\bar{t}\gamma$ production (including radiative top decays in $t\bar{t}$ events, solid line), the $t\bar{t}j$ background where one jet is misidentified as a photon (dotted line), the background from single-top production processes (dashed line), and the $W\gamma b\bar{b}jj$ background (histogram). The cuts imposed are listed in Eqs. (23)–(28). The photon misidentification probabilities used are described in the text. No particle ID efficiencies are included here.

Feynman diagrams contributing to $W\gamma b\bar{b}jj$ production. Numerical evaluation of these helicity amplitudes is very time consuming. We therefore show the $W\gamma b\bar{b}jj$ differential cross section in form of a histogram, where the error bars represent the statistical uncertainty of the Monte Carlo integration. The $t\bar{t}j$ background is seen to be a factor two to ten smaller than the $t\bar{t}\gamma$ signal for the jet-photon misidentification probabilities used. The sharp kink in the $t\bar{t}j$ differential cross section at the Tevatron is due to the functional form of $P_{j\to\gamma}$ (see Eq. (30)). The $(t\bar{b}\gamma + \bar{t}b\gamma) + X$ and $W\gamma b\bar{b}jj$ backgrounds both are found to be more than an order of magnitude smaller the $t\bar{t}j$ background.

The numerical results shown in Fig. 1 and all subsequent figures which display differential cross sections represent cross sections after selection cuts but *before* any particle identification efficiencies are taken into account.

It should be noted that the cross sections of the $t\bar{t}j$, the $(t\bar{b}\gamma + \bar{t}b\gamma) + X$, and the $W\gamma b\bar{b}jj$ backgrounds depend significantly on the choice of factorization and renormalization scales, μ_F and μ_R, which were taken to be $\mu_F = \mu_R = m_t$. Including next-to-leading oder (NLO) corrections in most cases significantly reduces the scale dependence of a process. Unfortunately the NLO QCD corrections are not presently known for any of the background processes. However, as we shall discuss in Sec. V C, it may be possible to extract the background cross sections using data. For the dominant $t\bar{t}j$ background this should provide a more accurate estimate of the cross section than the leading order QCD prediction.

Other reducible background sources are $t\bar{b}$ + 3 jet, $\bar{t}b$ + 3 jet, $t\bar{b}\ell^-\bar{\nu}j$, $\bar{t}b\ell^+\nu j$ and $Wb\bar{b}$ + 3 jet production, where one jet fakes a photon; $W\gamma$ + 4 jet production where two jets are misidentified as b jets; WW + 3 jet production where one jet fakes a photon and two jets are misidentified as b jets; and $Z\gamma b\bar{b}jj$ production where one of the leptons from the Z decay is lost (we implicitly mean Z/γ^* whenever the final state is dileptons). We find the combined cross section for the single-top + jet(s) processes to be about a factor ten smaller than that for $(t\bar{b}\gamma + \bar{t}b\gamma) + X$ production; similarly for the $Wb\bar{b}$ + 3 jet background. Since $P_{j\to b}$ is very small *and* we require two tagged b jets, the background from $W\gamma$ + 4 jet production where two jets are misidentified as b jets is negligible; so is the WW + 3 jet background. It should be noted that for a luminosity-upgraded LHC (SLHC), $P_{j\to b}$ may dramatically increase with as many as one in four light jets being misidentified as a b quark [47]. In this case, the $W\gamma$ + 4 jet cross section may be of the same order as that of $W\gamma b\bar{b}jj$.

Reducible $Z\gamma b\bar{b}jj$ production contributes to the background if one of the leptons from Z/γ^* decay is missed. We consider a lepton to be missed if it has $p_T < 10$ GeV or $|\eta| > 2.5$. If the lepton is within a cone of $\Delta R < 0.2$ from a detected lepton and has 1 GeV $< p_T <$ 10 GeV, the detected lepton is not considered isolated and we reject the event. In order to avoid the collinear singularity when the missed lepton is collinear with an observed lepton (which is relevant only if the the missed lepton has $p_T < 1$ GeV), we retain finite lepton masses in the calculation.

With several $\times 10^4$ Feynman diagrams contributing, $p\bar{p}^{(-)} \to Z\gamma b\bar{b}jj$ is sufficiently complicated that it requires approximation. To estimate the $Z\gamma b\bar{b}jj$ background we use a procedure similar to that described in Ref. [41]. We first calculate the ratio of the $W\gamma b\bar{b}$ and $W\gamma b\bar{b}jj$ cross sections. We then calculate the $Z\gamma b\bar{b}$ cross section (including $\gamma^* \to \ell^+\ell^-$ interference) where one of the leptons from Z/γ^* is missed, and scale it by the $W\gamma b\bar{b}jj$ and $W\gamma b\bar{b}$ cross section ratio. Since they entail QCD radiation from very similar subprocesses, the $Z\gamma b\bar{b}jj/Z\gamma b\bar{b}$ and $W\gamma b\bar{b}jj/W\gamma b\bar{b}$ cross section ratios are expected to be

approximately equal. At the Tevatron (LHC), we find that the estimated $Z\gamma b\bar{b}jj$ cross section is about a factor 7 (2) smaller than that of $W\gamma b\bar{b}jj$.

In addition to the backgrounds considered so far, $\gamma\ell\nu_\ell b\bar{b}jj$ events (or their fakes) may also be produced in double parton scattering (DPS), or from multiple interactions occurring from separate $p\overset{(-)}{p}$ collisions in the same bunch crossing at high-luminosity running. In principle, one can identify multiple interactions by a total visible energy measurement or by tracing some final particle tracks back to distinctly separate primary vertices, but this may not always be possible in practice. To estimate the cross sections from DPS and multiple interactions, we use the approximation outlined in Ref. [53]. At the LHC, the cross section from overlapping events is about a factor of 2 larger than that from DPS. At the Tevatron, for a luminosity of $\mathcal{L} = 10^{32}\text{cm}^{-2}\text{s}^{-1}$, DPS dominates. The resulting background arises predominantly from the overlap of a $t\bar{t}$ event and a two-jet event, wherein one jet is misidentified as a photon and the other is missed. We estimate the cross section for this process to be approximately 0.7 fb (0.01 fb) at the LHC (Tevatron), which is of the same order or smaller than for $W\gamma b\bar{b}jj$. The cross sections for the SM signal and the most important background processes are summarized in Table I.

As stated before, we require that both b quarks be tagged. Requiring only one tagged b quark would result in a signal cross section increase of a factor $(2/\epsilon_b - 1)$. This larger signal rate comes at the expense of an increased background and a reduced acceptance. In events where one of the b quarks is not tagged, photon radiation off the untagged b quark cannot be suppressed by a larger ΔR cut. Furthermore, to suppress the contributions from radiative W decay, the invariant mass cut on the $jj\gamma$ system in Eq. (24) has to be imposed on all three possible $jj\gamma$ combinations. This reduces the signal cross section by almost a factor 2. In addition, for events with only one b tag, the background will be larger. The $t\bar{t}j$ background increases by roughly 30% relative to the signal. The $(t\bar{b}\gamma + \bar{t}b\gamma) + X$ and $W\gamma b\bar{b}jj$ backgrounds increase due to the larger combinatorial background from grouping jets, the tagged b quark and the $\ell\nu$ system into $b\ell\nu(\gamma)$, $jjj(\gamma)$, $j\ell\nu(\gamma)$ and $bjj(\gamma)$ systems which are compatible with (radiative) top decay. Detailed calculations are needed for a quantitative estimate of the increase of these backgrounds. Finally, the $W\gamma + 4$ jet and $WW + 3$ jet backgrounds increase by about 2 orders of magnitude due to the much higher probability that only one (instead of two) light jet is mistagged as a b quark. Nevertheless, they are still expected to be far smaller than the $W\gamma b\bar{b}jj$ background. Since the single-b-tagged final state is less ''clean'' than that where both b quarks are identified, we do not consider it in detail here.

TABLE I. Expected cross sections (fb) for the $\gamma\ell\nu_\ell b\bar{b}jj$ signal and the most important background processes at the Tevatron and the LHC for the cuts described in Sec. III A. The photon misidentification probabilities used are described in the text. No particle ID efficiencies are included.

Process	Tevatron	LHC
signal	4.9	81.7
$t\bar{t}j$	0.78	45.7
$(t\bar{b}\gamma + \bar{t}b\gamma) + X$	0.03	2.64
$W\gamma b\bar{b}jj$	0.07	0.89
$Z\gamma b\bar{b}jj$	0.01	0.43
$t\bar{t} \oplus jj$	0.01	0.7

C. Signatures for anomalous $tt\gamma$ couplings

The photon transverse momentum distributions for $p\overset{(-)}{p} \to \gamma\ell\nu_\ell b\bar{b}jj$ in the SM and for various anomalous $tt\gamma$ couplings, together with the combined $p_T(\gamma)$ distribution of the $t\bar{t}j$, $W\gamma b\bar{b}jj$ and the $(t\bar{b}\gamma + \bar{t}b\gamma) + X$ backgrounds, are shown in Fig. 2. Only one coupling at a time is allowed to deviate from its SM prediction. At the Tevatron, the $\gamma\ell\nu_\ell b\bar{b}jj$ cross section is completely dominated by $q\bar{q}$ annihilation. As a result, photon radiation off the initial-state quarks constitutes an irreducible background which limits the sensitivity of the photon differential cross section to anomalous $tt\gamma$ couplings. This is particularly pronounced for F_{1V}^γ. Even when the photon does not couple to the top quark at all [$\Delta F_{1V}^\gamma = 2/3$ with all other $tt\gamma$ couplings vanishing; dashed line in Fig. 2(a)], the cross section hardly differs from the SM result. In contrast, at the LHC more than 75% of the $\gamma\ell\nu_\ell b\bar{b}jj$ cross section originates from gluon fusion. This results in a greatly-increased sensitivity of the $p_T(\gamma)$ distribution to nonstandard $tt\gamma$ couplings, which is evident from Fig. 2(b).

Nonstandard vector and axial vector couplings yield a transverse momentum distribution for the photon with high-p_T behavior similar to that in the SM. At low photon transverse momenta, however, the shape of the p_T distribution for SM and anomalous couplings differs. This is most easily noticed for $\Delta F_{1V}^\gamma = 1$ in Fig. 2(b). The change in shape at low p_T is due to radiative top decays which can contribute only in this region. Nonstandard and SM helicity amplitudes interfere differently for $t\bar{t}\gamma$ production and $t\bar{t}$ events where one of the top quarks decays radiatively, resulting in a shape change. Since the interference effects can be constructive or destructive, nonstandard vector or axial vector couplings can either increase or decrease the signal cross section.

Terms in the helicity amplitudes proportional to the dipole form factors $F_{2V,A}^\gamma$ grow like $m(t\gamma)/m_t$ at high energies. Here, $m(t\gamma)$ is the invariant mass of the photon and the top quark to which it couples. This results in a transverse momentum distribution of the photon which is considerably harder than that of a nonstandard vector or axial vector coupling. The long-dashed curves in Fig. 2 show the photon p_T distribution for $F_{2V}^\gamma = 3$ ($F_{2V}^\gamma = -1$)

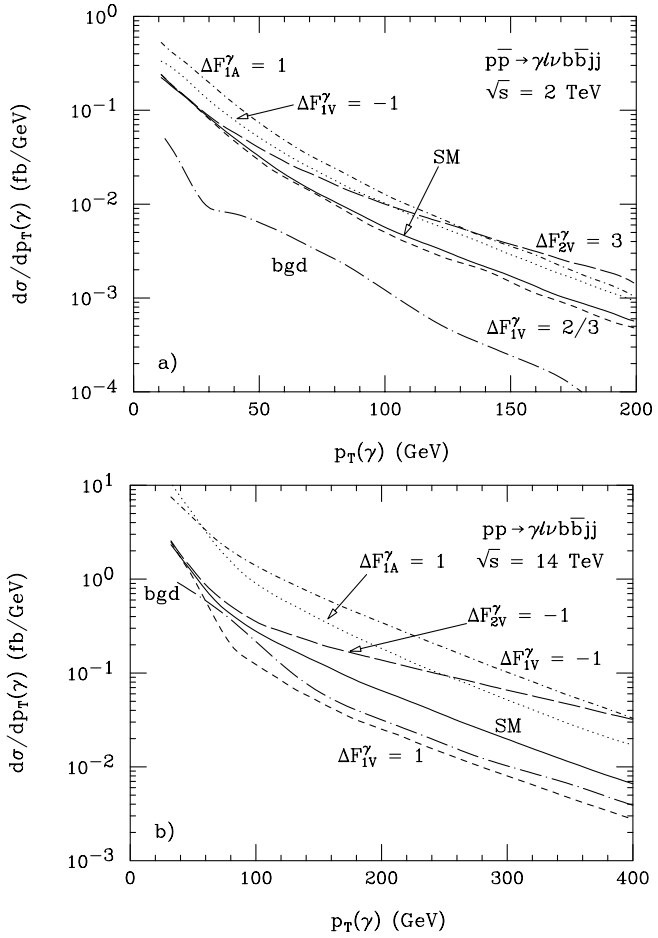

FIG. 2. The differential cross sections as a function of the photon transverse momentum for $\gamma\ell\nu_\ell b\bar{b}jj$ production at (a) Tevatron Run II and (b) LHC. Shown are the SM predictions for $t\bar{t}\gamma$ production (including radiative top decays in $t\bar{t}$ events, solid line), the combined $t\bar{t}j$, $W\gamma b\bar{b}jj$ and $(t\bar{b}\gamma + \bar{t}b\gamma) + X$ background (long-dashed-dotted line), and the predictions for several nonstandard $tt\gamma$ couplings. Only one coupling at a time is allowed to deviate from its SM value. The cuts imposed are listed in Eqs. (23)–(28). No particle ID efficiencies are included here.

at the Tevatron (LHC). For equal coupling strengths, the numerical results obtained for F^{γ}_{2A} are almost identical to those found for F^{γ}_{2V}. To discriminate F^{γ}_{2V} from F^{γ}_{2A}, one can take advantage of the CP-violating nature of F^{γ}_{2A} and use the asymmetry $A^{\mu}_{\rm cut}(p_{T\rm cut})$ introduced in Ref. [54].

Anomalous $tt\gamma$ couplings also affect the single resonant $(t\bar{b}\gamma + \bar{t}b\gamma) + X$ background. However, since the $(t\bar{b}\gamma + \bar{t}b\gamma) + X$ background is small, this has almost no effect on the overall signal to background ratio, so we do not include the anomalous couplings in these backgrounds.

IV. $t\bar{t}Z$ PRODUCTION

The process $p^{(-)}\bar{p} \to t\bar{t}Z$ leads to either $\ell'^+\ell'^-\ell\nu b\bar{b}jj$ or $\ell'^+\ell'^- b\bar{b} + 4j$ final states if the Z-boson decays leptonically and one of the W bosons decays hadronically. For both final states the leptonic Z decay provides an efficient trigger. If the Z boson decays into neutrinos and both W bosons decay hadronically, the final state consists of $\not{p}_T b\bar{b} + 4j$. In this case one has to trigger on the multijet system, similar to many supersymmetry searches. For $Z \to \bar{\nu}\nu$ and one of the W bosons decaying leptonically, the $t\bar{t}$ background swamps the signal. Finally, for $Z \to jj(b\bar{b})$, $t\bar{t}jj$ $(t\bar{t}b\bar{b})$ production constitutes an overwhelming irreducible background.

In the following, we concentrate on the $\ell'^+\ell'^-\ell\nu b\bar{b}jj$ and $\ell'^+\ell'^- b\bar{b} + 4j$ final states, which we henceforth refer to as the trilepton and dilepton channels for brevity. The $\ell'^+\ell'^-\ell\nu\ell''\nu'' b\bar{b}$ channel, while experimentally cleaner, has a much smaller BR, so we ignore it. Because of the larger $Z \to \bar{\nu}\nu$ BR, the $\not{p}_T b\bar{b} + 4j$ channel cross section before cuts is about a factor 3 larger than that for the trilepton and dilepton final states. However, $t\bar{t}$ production with all-hadronic decays where one or more jets are badly mismeasured, and $t\bar{t}W$ production where the lepton from W decay is lost, constitute potentially large backgrounds. For this reason, we also do not consider the $\not{p}_T b\bar{b} + 4j$ final state here.

The signal cross section calculation proceeds similar to that in Sec. III. As in that case, form factor effects turn out to unimportant and are ignored. We assume real ttZ couplings. As with $t\bar{t}\gamma$ we include all decay spin correlations and finite width effects. Here we also include off-shell photon interference effects with $Z \to \ell'^+\ell'^-$. We take into account all top quark-resonant Feynman diagrams contributing to the trilepton and dilepton final states, including those where the final state W boson couples to ℓ'. To ensure gauge invariance of the SM result, we again use the overall-factor scheme.

A. The $t\bar{t}Z$ trilepton final state

In order to identify leptons, b quarks, light jets and the missing transverse momentum in $\ell'^+\ell'^-\ell\nu b\bar{b}jj$ events, we impose the cuts listed in Eq. (23). In addition, we require that there is a same-flavor, opposite-sign lepton pair with invariant mass near the Z resonance,

$$m_Z - 10\ \text{GeV} < m(\ell\ell) < m_Z + 10\ \text{GeV}. \qquad (31)$$

As a result of this final state signature requirement, $t\bar{t}Z$ production as observed is very insensitive to anomalous $tt\gamma$ couplings. Since there is essentially no phase space for $t \to WZb$ decays ($BR(t \to WZb) \approx 3 \cdot 10^{-6}$ [55,56]), this trilepton final state arises only from $t\bar{t}Z$ production. Thus, in addition to the cuts listed in Eqs. (23) and (31), we require that events satisfy Eq. (26), i.e., that the $b\ell\nu$ and bjj systems are consistent with top decay.

The main backgrounds contributing to the trilepton final state are singly-resonant $(t\bar{b}Z + \bar{t}bZ) + X$ ($t\bar{b}Zjj$, $\bar{t}bZjj$, $t\bar{b}Z\ell\nu$ and $\bar{t}bZ\ell\nu$) and nonresonant $WZb\bar{b}jj$ production.

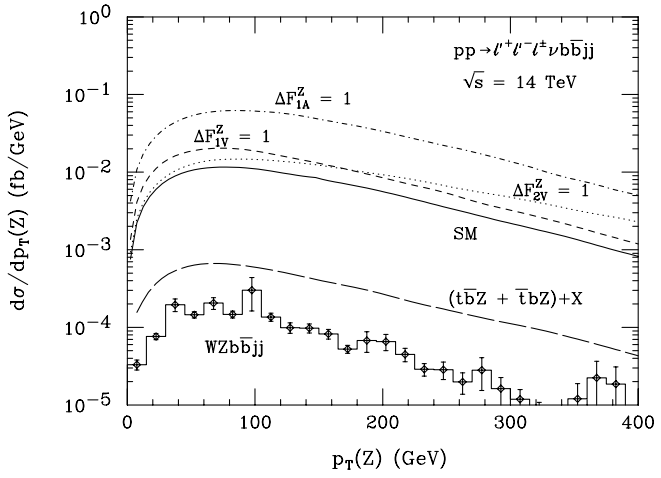

FIG. 3. The differential cross sections at the LHC as a function of $p_T(Z)$ for $\ell'^+\ell'^-\ell\nu b\bar{b}jj$ final states. Shown are the SM predictions for $t\bar{t}Z$ production (solid), the single-top background (dashed), the $WZb\bar{b}jj$ background (histogram), and the predictions for several nonstandard ttZ couplings. Only one coupling at a time is allowed to deviate from its SM value. The cuts imposed are listed in Eqs. (23), (26), and (31).

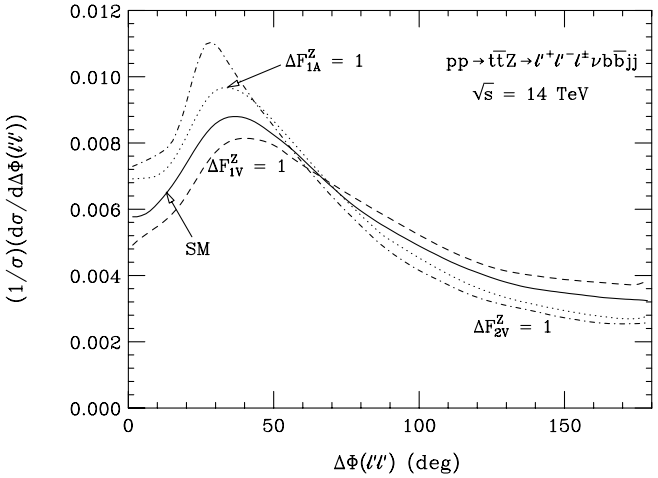

FIG. 4. The normalized differential signal cross sections at LHC as a function of the opening angle of the $Z \to \ell'^+\ell'^-$ leptons in the transverse plane, $\Delta\Phi(\ell'\ell')$. Shown are the SM distribution (solid line) and the predictions for several nonstandard ttZ couplings. Only one coupling at a time is allowed to deviate from its SM prediction. The cuts imposed are listed in Eqs. (23), (26), and (31).

As in the $t\bar{t}\gamma$ case, backgrounds from DPS and overlapping events are found to be negligible.

At the Tevatron, $t\bar{t}Z$ production is quite small, and the trilepton final state cross section is only about 0.02 fb, far too small to be observable for the anticipated integrated luminosity in Run II. We therefore consider this signature only for the LHC. The Z boson transverse momentum distribution is shown in Fig. 3 for the SM signal and backgrounds, as well as for the signal with several nonstandard ttZ couplings. Only one coupling at a time is allowed to deviate from its SM prediction. The backgrounds are each more than 1 order of magnitude smaller than the SM signal. As in $W\gamma b\bar{b}jj$ production, numerical evaluation of the $WZb\bar{b}jj$ helicity amplitudes is very time consuming. We thus show its differential cross section as a histogram, where the error bars represent the Monte Carlo statistical uncertainty.

Figure 3 shows that, as in the $tt\gamma$ case, the dimension-five couplings $F^Z_{2V,A}$ lead to a significantly harder transverse momentum distribution. Furthermore, as in the case of F^γ_{2V} and F^γ_{2A}, almost identical numerical results for F^Z_{2V} and F^Z_{2A} are found for equal coupling strengths, and a CP-violating asymmetry similar to $A^\mu_{\rm cut}(p_{T\rm cut})$ has to be used to discriminate between the weak magnetic and weak electric dipole form factors.

Varying $F^Z_{1V,A}$ leads mostly to a cross section normalization change, hardly affecting the shape of the $p_T(Z)$ distribution. This is because, unlike in the $tt\gamma$ case, there is no radiative top decay, i.e., no $t\bar{t}$ events where $t \to WZb$. This implies that, for the cuts we impose, the $p_T(Z)$ distribution for SM couplings and for $F^Z_{1V,A} = -F^{Z,SM}_{1V,A}$ are almost degenerate.

Currently, the SM $t\bar{t}Z$ cross section is known only at LO, and has substantial factorization and renormalization scale uncertainty. Since the backgrounds are insignificant, this normalization uncertainty will ultimately be the limiting factor in extracting anomalous vector and axial vector ttZ couplings, which mostly just change the normalization. To improve sensitivity to $F^Z_{1V,A}$, we need an observable which changes shape in the presence of anomalous couplings. An excellent candidate is the opening angle of the $Z \to \ell'^+\ell'^-$ leptons in the transverse plane, $\Delta\Phi(\ell'\ell')$. We show its normalized distribution for the SM and various anomalous couplings in Fig. 4. Anomalous vector couplings (dashed line) reduce the peaking at small opening angles, whereas the opposite is true for nonstandard axial vector couplings (dotted line). The shape change is most pronounced for $F^Z_{2V,A}$. Since the $p_T(Z)$ distribution is considerably harder in the presence of these couplings, the increased Z boson Lorentz boost leads to a decrease of $\Delta\Phi(\ell'\ell')$.

B. The $t\bar{t}Z$ dilepton final state

As in the trilepton case, we impose the cuts of Eq. (23) to identify leptons, b quarks and light jets, and again require that the $\ell'^+\ell'^-$ invariant mass satisfies Eq. (31). The main background arises from $Zb\bar{b} + 4j$ production, which we calculate using ALPGEN [57]. To adequately suppress it, we additionally require that events have at least one combination of jets and b quarks which fulfills the requirements

$$\begin{aligned} m_t - 20\ \text{GeV} < m(b_1 j_1 j_2) < m_t + 20\ \text{GeV}, \\ M_W - 20\ \text{GeV} < m(j_1 j_2) < M_W + 20\ \text{GeV}, \end{aligned} \tag{32}$$

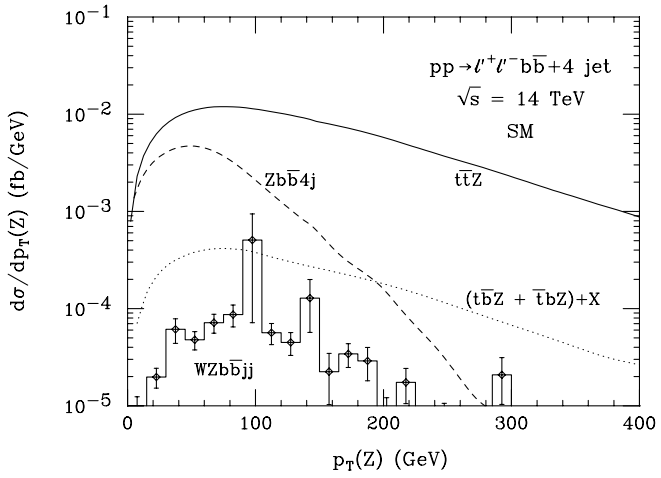

FIG. 5. The differential cross sections at the LHC as a function of $p_T(Z)$ for $\ell'^+\ell'^- b\bar{b} + 4j$ final states. The SM is the solid curve. Backgrounds are $Zb\bar{b} + 4j$ (dashed), single-top production (dotted), and $WZb\bar{b}jj$ (histogram). The cuts imposed are listed in Eqs. (23) and (31)–(33).

$$\begin{aligned} m_t - 20\ \text{GeV} < m(b_2 j_3 j_4) < m_t + 20\ \text{GeV}, \\ M_W - 20\ \text{GeV} < m(j_3 j_4) < M_W + 20\ \text{GeV}, \end{aligned} \tag{33}$$

where $b_{1,2} = b, \bar{b}$, and j_i, $i = 1, \ldots, 4$, are the four light jets. The SM $p_T(Z)$ distribution, together with those of the $Zb\bar{b} + 4j$, singly-resonant $(t\bar{b}Z + \bar{t}bZ) + X$ and nonresonant $WZb\bar{b}jj$ backgrounds is shown in Fig. 5. The signatures for anomalous ttZ couplings are similar to those in the trilepton channel, so we do not show them here.

The nonresonant backgrounds fall much faster with $p_T(Z)$ than the signal and singly-resonant background. The $Zb\bar{b} + 4j$ background is important only for $p_T(Z) < 100$ GeV. For $p_T(Z) > 200$ GeV, $(t\bar{b}Z + \bar{t}bZ) + X$ production constitutes the largest background. Except for very small values of $p_T(Z)$, the signal to background ratio (S:B) is significantly better than 1:1. The SM signal cross section is approximately the same size as in the dilepton final state. We therefore take both channels into account in extracting anomalous coupling sensitivity limits. Cross sections for the signal and backgrounds are summarized in Table II.

TABLE II. Expected LHC cross sections (fb) for the $t\bar{t}Z$ trilepton and dilepton channels. The cuts applied are described in the text. No particle ID efficiencies are included.

Process	$\ell'^+\ell'^-\ell\nu b\bar{b}jj$	$\ell'^+\ell'^- b\bar{b} + 4j$
signal	2.25	2.32
$Zb\bar{b}$ + 4 jet	–	0.43
$(t\bar{b}Z + \bar{t}bZ) + X$	0.12	0.08
$WZb\bar{b}jj$	0.03	0.02

V. LIMITS ON ANOMALOUS TOP QUARK COUPLINGS

The shape and normalization changes of the photon or Z-boson transverse momentum distribution and, for $t\bar{t}Z$ production, the $\Delta\Phi(\ell'\ell')$ distribution, can be used to derive quantitative sensitivity bounds on the anomalous $tt\gamma$ and ttZ couplings. We do this by performing a χ^2 test on the distributions and calculating 68% and 95% confidence level (CL) limits. To calculate the statistical significance, we split the distributions into a number of bins, each with typically more than five events, approximating the Poisson statistics via a Gaussian distribution. We impose the cuts described in Secs. III and IV and combine channels with electrons and muons in the final state, conservatively assuming a common lepton identification efficiency of $\epsilon_\ell = 0.85$ for each lepton. We take the identification efficiency for photons to be $\epsilon_\gamma = 0.8$ and assume a double b-tag efficiency of $\epsilon_b^2 = 0.25(0.4)$ at the Tevatron (LHC). Except for the $tt\gamma$ and ttZ couplings we assume the SM to be valid: the Wtb and ttg couplings can be precisely measured at the LHC in single-top [14] and $t\bar{t}$ production [58]. Correlations between different anomalous couplings are fully included.

Our expression for the χ^2 statistics used to compute confidence levels is [59]

$$\chi^2 = \sum_{i=1}^{n_D} \frac{(N_i - f N_i^0)^2}{f N_i^0} + (n_D - 1), \tag{34}$$

where n_D is the number of bins, N_i is the number of events for a given set of anomalous couplings, and N_i^0 is the number of events in the SM in the ith bin. The parameter f reflects the uncertainty in SM cross section normalization within the allowed range. We determine it by minimizing χ^2:

$$f = \begin{cases} (1 + \Delta\mathcal{N})^{-1} & \text{for} \quad \bar{f} < (1 + \Delta\mathcal{N})^{-1} \\ \bar{f} & \text{for} \quad (1 + \Delta\mathcal{N})^{-1} < \bar{f} < 1 + \Delta\mathcal{N} \\ 1 + \Delta\mathcal{N} & \text{for} \quad \bar{f} > 1 + \Delta\mathcal{N} \end{cases} \tag{36}$$

with

$$\bar{f}^{\,2} = \left\{ \sum_{i=1}^{n_D} N_i^0 \right\}^{-1} \sum_{i=1}^{n_D} \frac{N_i^2}{N_i^0}. \tag{39}$$

The parameter $\Delta\mathcal{N}$ is the SM cross section uncertainty. It arises primarily from the currently-unknown signal QCD corrections, and from PDF uncertainties. In the following we assume $\Delta\mathcal{N} = 30\%$ unless stated otherwise. We universally assume real anomalous couplings.

A. Sensitivity bounds for $tt\gamma$ couplings

To derive sensitivity bounds for anomalous $tt\gamma$ couplings, we take into account the $t\bar{t}j$, singly-resonant $(t\bar{b}\gamma + \bar{t}b\gamma) + X$, and $W\gamma b\bar{b}jj$ backgrounds. The variation of the

singly-resonant background with $tt\gamma$ anomalous couplings is ignored. For the probabilities that a jet fakes a photon at the Tevatron and LHC we use the values listed in Sec. III B. All other backgrounds are assumed to be negligible. For the Tevatron, we derive sensitivity limits for an integrated luminosity of 8 fb^{-1} which is the total integrated luminosity anticipated for Run II. For the LHC we calculate bounds for 30 fb^{-1}, 300 fb^{-1}, and 3000 fb^{-1}. An integrated luminosity of 300 fb^{-1} corresponds to 3 years of running at the LHC design luminosity of $\mathcal{L} = 10^{34}\text{cm}^{-2}s^{-1}$. The smaller value of 30 fb^{-1} is expected for the first few years of operation of the LHC when the luminosity is likely to be significantly smaller than design. The larger value of 3000 fb^{-1} can be achieved in about three years of running at a luminosity-upgraded LHC.

Our results for the Tevatron are shown in Table III. The correlations between various anomalous $tt\gamma$ couplings are illustrated in Fig. 6 for two combinations, ΔF^{γ}_{1V} versus ΔF^{γ}_{1A}, and ΔF^{γ}_{1A} versus ΔF^{γ}_{2A}. Correlations between the couplings are seen to be fairly small at Tevatron energies. This is also the case for the combinations not shown.

Because of the small cross section and the complicating "background" from photon radiation off initial-state quarks, Tevatron experiments are essentially insensitive to the dipole form factors $F^{\gamma}_{2V,A}$. The achievable bounds for these are worse than the limits from S-matrix unitarity for a form factor scale $\Lambda_{FF} \geq 1$ TeV. However, for the $tt\gamma$ vector and axial vector couplings, which are not (directly or indirectly) constrained by any existing experiment, CDF and DØ will be able to perform a first, albeit not very precise, measurement. The prospects are most favorable for F^{γ}_{1A}, which, as shown in Table III, can be determined with an accuracy of about 70% for a SM cross section normalization uncertainty of 30%.

As shown in Fig. 6(a), the precision on F^{γ}_{1A} can be improved to about 50% if the normalization uncertainty can be reduced to 10%. This depends critically on the signal normalization. Currently, the $t\bar{t}\gamma$ cross section is known only at LO. Once the NLO QCD corrections are known, a 10% normalization uncertainty may be realistic.

TABLE III. Sensitivities achievable at 68.3% and 95% CL for anomalous $tt\gamma$ couplings in $p\bar{p} \to \gamma\ell\nu_\ell b\bar{b}jj$ at the Tevatron ($\sqrt{s} = 2$ TeV) for an integrated luminosity of 8 fb^{-1}. The limits shown represent the maximum and minimum values obtained when taking into account the correlations between any possible pair of anomalous couplings. The cuts imposed are described in Sec. III A.

Coupling	68.3% CL	95% CL
ΔF^{γ}_{1V}	$^{+1.92}_{-1.20}$	$^{+2.60}_{-1.88}$
ΔF^{γ}_{1A}	$^{+0.69}_{-0.82}$	$^{+1.03}_{-1.17}$
ΔF^{γ}_{2V}	$^{+5.16}_{-5.21}$	$^{+8.49}_{-8.73}$
ΔF^{γ}_{2A}	$^{+5.19}_{-5.08}$	$^{+7.85}_{-8.43}$

The bound on F^{γ}_{1A} can, in principle, be further tightened by enlarging the signal sample by requiring only one b-tagged jet. As mentioned before, the increase in signal statistics when including single tagged events comes at the price of increased background. To quantify the improvement, detailed simulations are needed.

The sensitivity bounds achievable at the LHC are shown in Table IV and Fig. 7. Even for a modest integrated luminosity of 30 fb^{-1}, one expects more than 500 signal events after acceptances and efficiencies are taken into account. This will make it possible to measure the $tt\gamma$ vector and axial vector couplings, and the dipole form factors, with a precision of typically 20% and 35%, respectively. For 300 fb^{-1}, the limits improve to $4 - 7\%$ for $F^{\gamma}_{1V,A}$ and to about 20% for $F^{\gamma}_{2V,A}$. At the SLHC, assuming

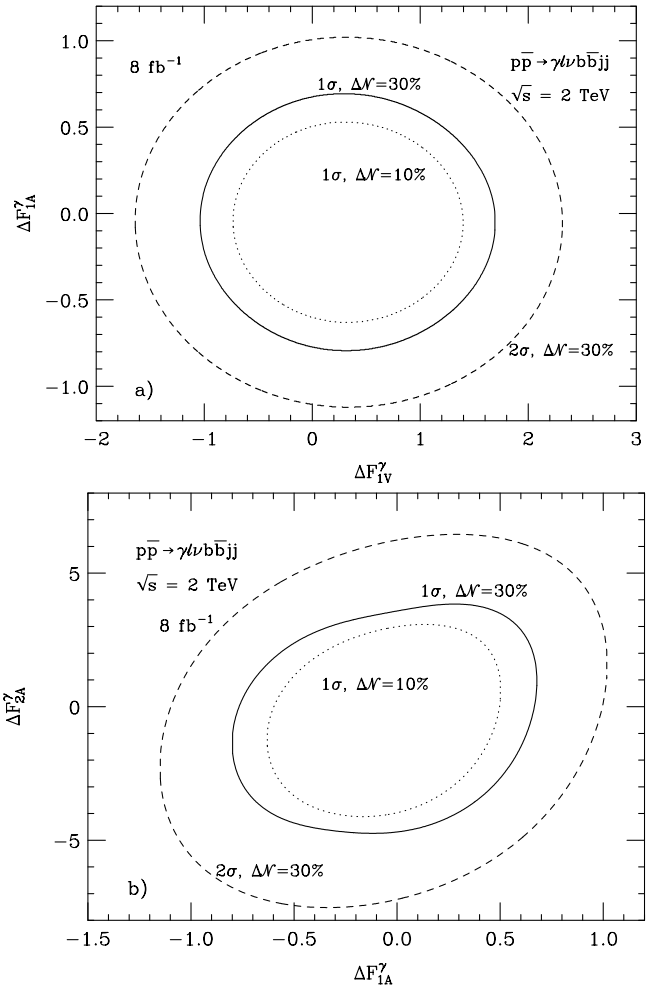

FIG. 6. Projected bounds on anomalous $tt\gamma$ couplings for $p\bar{p} \to \gamma\ell\nu_\ell b\bar{b}jj$ at the Tevatron and an integrated luminosity of 8 fb^{-1}. Shown are 68.3% (solid) and 95% CL limits (dashed) for a SM cross section normalization uncertainty of $\Delta\mathcal{N} = 30\%$, and the 68.3% CL limits for $\Delta\mathcal{N} = 10\%$: (a) for ΔF^{γ}_{1A} versus ΔF^{γ}_{1V}; and (b) for ΔF^{γ}_{2A} versus ΔF^{γ}_{1A}. In each graph, only those couplings which are plotted against each other are assumed to be different from their SM values.

TABLE IV. Sensitivities achievable at 68.3% CL for anomalous $tt\gamma$ couplings in $pp \to \gamma\ell\nu_\ell b\bar{b}jj$ at the LHC ($\sqrt{s} = 14$ TeV) for an integrated luminosities of 30 fb^{-1}, 300 fb^{-1}, and 3000 fb^{-1}. The limits shown represent the maximum and minimum values obtained when taking into account the correlations between any possible pair of anomalous couplings. The cuts imposed are described in Sec. III A.

Coupling	30 fb^{-1}	300 fb^{-1}	3000 fb^{-1}
ΔF^γ_{1V}	$^{+0.23}_{-0.14}$	$^{+0.079}_{-0.045}$	$^{+0.037}_{-0.019}$
ΔF^γ_{1A}	$^{+0.17}_{-0.52}$	$^{+0.051}_{-0.077}$	$^{+0.018}_{-0.024}$
ΔF^γ_{2V}	$^{+0.34}_{-0.35}$	$^{+0.19}_{-0.20}$	$^{+0.12}_{-0.12}$
ΔF^γ_{2A}	$^{+0.35}_{-0.36}$	$^{+0.19}_{-0.21}$	$^{+0.11}_{-0.14}$

an integrated luminosity of 3000 fb^{-1}, one can hope to achieve a $2-3\%$ measurement of the vector and axial vector couplings, and a 10% measurement of $F^\gamma_{2V,A}$, provided that particle identification efficiencies are not substantially smaller, and the reducible backgrounds not much larger, than what we have assumed.

As shown in Fig. 7, with the exception of F^γ_{2V} and F^γ_{2A} [see Fig. 7(d)], there are substantial correlations between the $tt\gamma$ couplings at the LHC, in particular, for low integrated luminosities where small changes in the shape of the $p_T(\gamma)$ distribution are not resolved with the available statistics. Varying only one coupling at a time thus will produce overly optimistic limits. The correlations between F^γ_{2V} and F^γ_{1A} (F^γ_{2A} and F^γ_{1V}) are similar to those for F^γ_{2A} and F^γ_{1A} (F^γ_{2V} and F^γ_{1V}) and thus not shown in Fig. 7. In contrast to the Tevatron, the bounds on the $tt\gamma$ couplings at the LHC vary only slightly with the normalization uncertainty if $\Delta\mathcal{N}$ is between 10% and 30%.

B. Sensitivity bounds for ttZ couplings

To extract bounds on the ttZ couplings, we perform a simultaneous fit to the $p_T(Z)$ and the $\Delta\Phi(\ell'\ell')$ distributions, using both the trilepton and dilepton final states. Since the $(t\bar{b}Z + \bar{t}bZ) + X$ and $WZb\bar{b}jj$ backgrounds are very small, we take only the $Zb\bar{b} + 4j$ background into account in our χ^2 analysis. We calculate sensitivity bounds

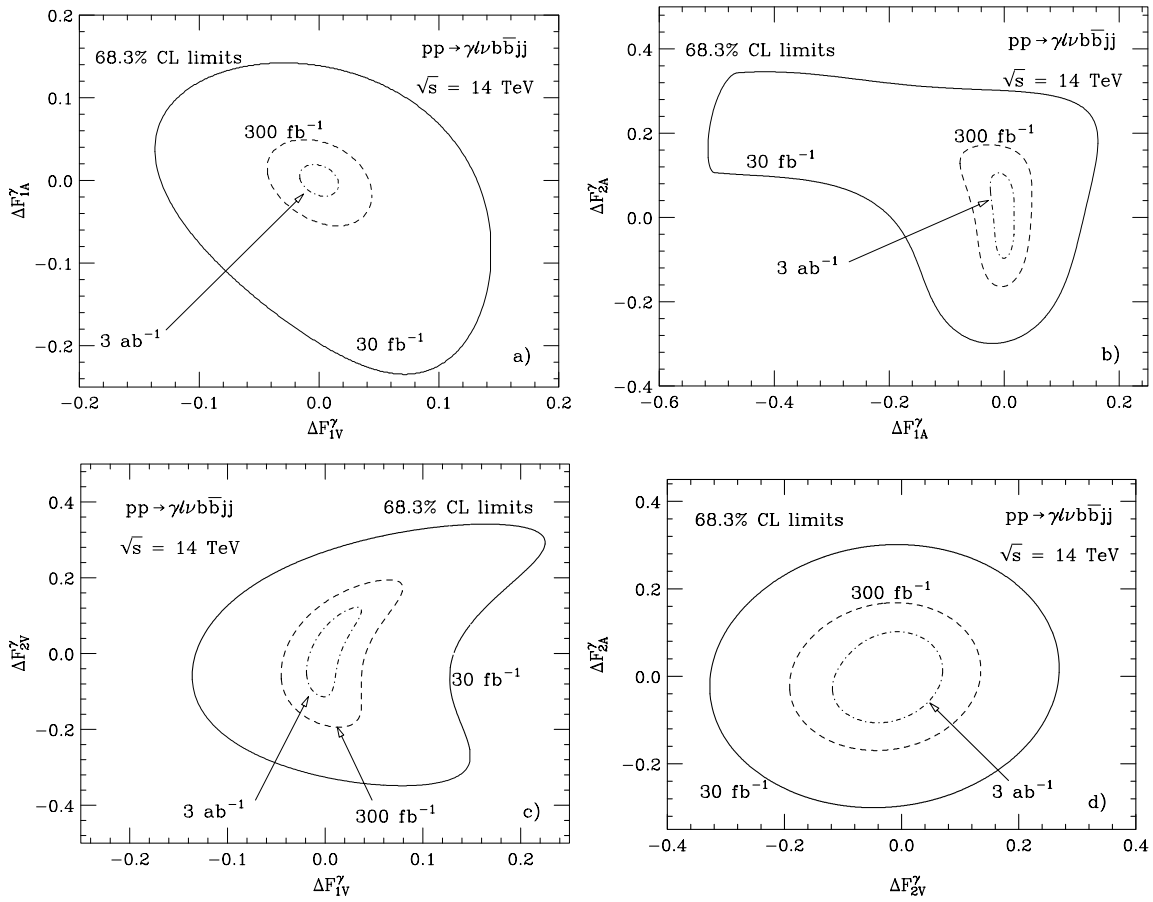

FIG. 7. Projected bounds on anomalous $tt\gamma$ couplings for $pp \to \gamma\ell\nu_\ell b\bar{b}jj$ at the LHC. Shown are 68.3% CL limits for a SM cross section normalization uncertainty of $\Delta\mathcal{N} = 30\%$ and for integrated luminosities of 30 fb^{-1} (solid), 300 fb^{-1} (dashed), and 3000 fb^{-1} (dot-dashed): (a) for ΔF^γ_{1A} versus ΔF^γ_{1V}, (b) for ΔF^γ_{2A} versus ΔF^γ_{1A}, (c) for ΔF^γ_{2V} versus ΔF^γ_{1V} and (d) for ΔF^γ_{2A} versus ΔF^γ_{2V}. In each graph, only those couplings which are plotted against each other are assumed to be different from their SM values.

TABLE V. Sensitivities achievable at 68.3% CL for anomalous ttZ couplings at the LHC for integrated luminosities of 300 fb^{-1}, and 3000 fb^{-1}. The limits shown represent the maximum and minimum values obtained when taking into account the correlations between any possible pair of anomalous couplings. The cuts imposed are described in Secs. III A and IV A.

Coupling	300 fb^{-1}	3000 fb^{-1}
ΔF_{1V}^Z	$^{+0.87}_{-0.46}$	$^{+0.62}_{-0.22}$
ΔF_{1A}^Z	$^{+0.15}_{-0.20}$	$^{+0.056}_{-0.074}$
ΔF_{2V}^Z	$^{+0.52}_{-0.52}$	$^{+0.30}_{-0.29}$
ΔF_{2A}^Z	$^{+0.54}_{-0.53}$	$^{+0.30}_{-0.31}$

for 300 fb^{-1} and 3000 fb^{-1} at the LHC; for 30 fb^{-1} the number of events expected is too small to yield meaningful results.

Our results are shown in Table V and Fig. 8. For an integrated luminosity of 300 fb^{-1}, it will be possible to measure the ttZ axial vector coupling with a precision of $15-20\%$, and $F_{2V,A}^Z$ with a precision of $50-55\%$. At the SLHC, these bounds can be improved by factors of about 1.6 ($F_{2V,A}^Z$) and 3.0 (F_{1A}^Z). The bounds which can be achieved for F_{1V}^Z are much weaker than those projected for F_{1A}^Z. As mentioned in Sec. IV B, the $p_T(Z)$ distributions for the SM and for $F_{1V,A}^Z = -F_{1V,A}^{Z,SM}$ are almost degenerate. This is also the case for the $\Delta\Phi(\ell'\ell')$ distribution. In a fit to these two distributions, therefore, an area centered at $\Delta F_{1V,A}^Z = -2F_{1V,A}^{Z,SM}$ remains which cannot be excluded, even at the SLHC where one expects several thousand $t\bar{t}Z$ events. For F_{1V}^Z, the two regions merge, resulting in rather poor limits. For F_{1A}^Z, the two regions are distinct. Since the area centered at $\Delta F_{1A}^Z = -2F_{1A}^{Z,SM}$ is incompatible with the indirect limits on the ttZ vector and axial vector couplings from LEP data, it is not included in Table V or Fig. 8.

The bounds on the ttZ couplings, with the exception of F_{2V}^Z and F_{1A}^Z [see Fig. 8(b)], are not strongly correlated. The correlations between F_{2V}^Z and F_{1A}^Z (F_{2A}^Z and F_{1V}^Z) are

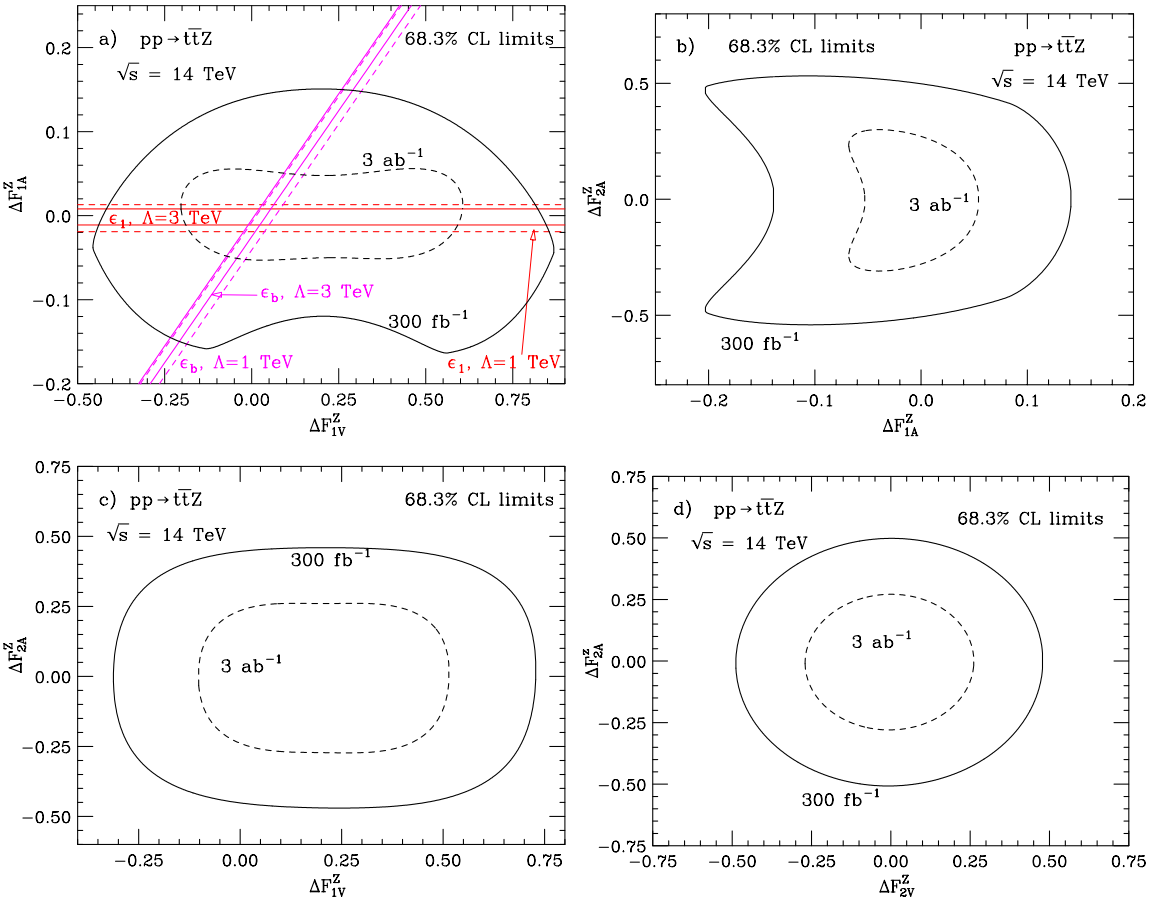

FIG. 8 (color online). Projected bounds on anomalous ttZ couplings for at the LHC. Shown are 68.3% CL limits for integrated luminosities of 300 fb^{-1} (solid) and 3000 fb^{-1} (dashed): (a) for ΔF_{1A}^Z versus ΔF_{1V}^Z, (b) for ΔF_{2A}^Z versus ΔF_{1A}^Z, (c) for ΔF_{2V}^Z versus ΔF_{1V}^Z and (d) for ΔF_{2A}^Z versus ΔF_{2V}^Z. In (a) we also include the (indirect) constraints from LEP data (see Eqs. (17) and (18)) for two choices of the loop momentum cutoff scale Λ (solid: $\Lambda = 3$ TeV, dashed: $\Lambda = 1$ TeV). In each graph, only those couplings which are plotted against each other are assumed to be different from their SM values.

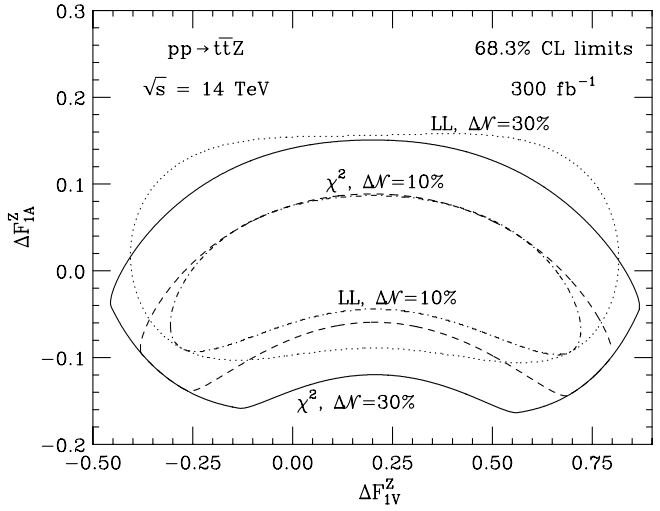

FIG. 9. Projected 68.3% CL bounds on ΔF^Z_{1A} and ΔF^Z_{1V} for 300 fb^{-1} at the LHC. The solid and dashed curves show the sensitivity bounds obtained using the χ^2 test described at the beginning of this section for $\Delta\mathcal{N} = 30\%$ and $\Delta\mathcal{N} = 10\%$, respectively. The dotted and dot-dashed lines correspond to the limits found using the log-likelihood method. All other ttZ couplings are assumed to have their SM values.

similar to those for F^Z_{2A} and F^Z_{1A} (F^Z_{2V} and F^Z_{1V}) and thus are not shown. In Fig. 8(a) we also include the indirect bounds resulting from LEP data (see Eqs. (17) and (18)) for two choices of the loop momentum cutoff scale Λ.

To test the robustness of our sensitivity limits for anomalous ttZ couplings, we have performed an independent analysis using Poisson statistics and the log-likelihood method. The normalization uncertainty in this approach is treated as a Gaussian fluctuation with standard deviation $\Delta\mathcal{N}$. Except for F^Z_{1A}, the limits obtained using the log-likelihood method are similar to those shown in Table V and Fig. 8; they are typically $5 - 10\%$ more stringent. For the ttZ axial vector coupling we observe a somewhat larger variation. The same statement also holds for the sensitivity of the bounds on the normalization uncertainty $\Delta\mathcal{N}$. This is illustrated in Fig. 9, where we show 68.3% CL limits for ΔF^Z_{1A} versus ΔF^Z_{1V} and 300 fb^{-1} at the LHC, using the χ^2 test described at the beginning of this section (solid and dashed lines), and the log-likelihood method (dotted and dot-dashed lines). For both methods, results are shown for $\Delta\mathcal{N} = 30\%$, and $\Delta\mathcal{N} = 10\%$. The sensitivity bounds on ΔF^Z_{1A} are seen to vary by as much as 50% with the statistical method employed, and can be improved by as much as factor 2 if $\Delta\mathcal{N}$ can be reduced from 30% to 10%. As in the $t\bar{t}\gamma$ case, a 10% normalization uncertainty may be realistic once the NLO QCD corrections to $t\bar{t}Z$ production are known.

C. Discussion

It is instructive to compare the bounds for anomalous ttV couplings achievable at hadron colliders with the indirect limits from LEP data and $b \to s\gamma$ decays, and with those projected for a future e^+e^- linear collider. The $tt\gamma$ vector and axial vector couplings are unconstrained by LEP and $b \to s\gamma$ data. Thus, the Tevatron offers a first opportunity to probe these couplings, although the sensitivity is severely limited by statistics and the background from initial-state radiation. A much more precise measurement can be performed at the LHC, which will also be able to determine the dipole form factors $F^\gamma_{2V,A}$ at the $10 - 20\%$ level. Comparing the bounds on F^γ_{2V} (Table IV) with the indirect limits derived in Sec. II C, one observes that the LHC (SLHC) can improve the current bound from $b \to s\gamma$ decays by a factor of about 2 (5). On the other hand, the limits on F^γ_{2A} which one expects at the LHC are at least 1 order of magnitude more stringent than those from $b \to s\gamma$, if one assumes F^γ_{2A} to be real.

The ϵ_1 and ϵ_b parameters constrain the ttZ vector and axial vector couplings to within a few-percent of their SM values if one assumes that no other source of new physics contributes to these parameters. Table V and Fig. 8(a) show that it will be impossible to match that precision at the LHC, even for an integrated luminosity of 3000 fb^{-1}. In contrast, ϵ_2 and ϵ_3 only constrain a linear combination of F^Z_{2V} and F^γ_{2V}. Thus, $t\bar{t}Z$ production at the LHC will provide valuable information on the dimension-five ttZ couplings.

The most complete study of $t\bar{t}$ production at a future e^+e^- linear collider for general ttV ($V = \gamma, Z$) couplings so far is that of Ref. [20]. It uses the parametrization of Eq. (5) for the ttV vertex function. In order to compare the bounds of Ref. [20] with those anticipated at the LHC, the limits derived in Secs. V A and V B have to be converted into bounds on $\tilde{F}^V_{1V,A}$ and $\tilde{F}^V_{2V,A}$ (see Eqs. (6)–(9)). Table VI compares the bounds we obtain for $\tilde{F}^V_{1V,A}$ and $\tilde{F}^V_{2V,A}$ with those reported in Ref. [20] for an e^+e^- linear collider operating at $\sqrt{s} = 500$ GeV, which assumes a linear polarization of $\mathcal{P}^- = \mathcal{P}^+ = 0.8$ for both electron and positron

TABLE VI. Sensitivities achievable at 68.3% CL for the anomalous ttV ($V = \gamma, Z$) couplings $\tilde{F}^V_{1V,A}$ and $\tilde{F}^V_{2V,A}$ of Eq. (5) at the LHC for integrated luminosities of 300 fb^{-1}, and at an e^+e^- linear collider operating at $\sqrt{s} = 500$ GeV (taken from Ref. [20]). Only one coupling at a time is allowed to deviate from its SM value.

Coupling	LHC, 300 fb^{-1}	e^+e^- [20]
$\Delta\tilde{F}^\gamma_{1V}$	$^{+0.043}_{-0.041}$	$^{+0.047}_{-0.047}$, 200 fb^{-1}
$\Delta\tilde{F}^\gamma_{1A}$	$^{+0.051}_{-0.048}$	$^{+0.011}_{-0.011}$, 100 fb^{-1}
$\Delta\tilde{F}^\gamma_{2V}$	$^{+0.038}_{-0.035}$	$^{+0.038}_{-0.038}$, 200 fb^{-1}
$\Delta\tilde{F}^\gamma_{2A}$	$^{+0.16}_{-0.17}$	$^{+0.014}_{-0.014}$, 100 fb^{-1}
$\Delta\tilde{F}^Z_{1V}$	$^{+0.43}_{-0.83}$	$^{+0.012}_{-0.012}$, 200 fb^{-1}
$\Delta\tilde{F}^Z_{1A}$	$^{+0.14}_{-0.14}$	$^{+0.013}_{-0.013}$, 100 fb^{-1}
$\Delta\tilde{F}^Z_{2V}$	$^{+0.38}_{-0.50}$	$^{+0.009}_{-0.009}$, 200 fb^{-1}
$\Delta\tilde{F}^Z_{2A}$	$^{+0.50}_{-0.51}$	$^{+0.052}_{-0.052}$, 100 fb^{-1}

beams. Ref. [20] lists sensitivity bounds only for the case that only one coupling at a time is allowed to deviate from its SM value, as we do for the LHC in Table VI. Furthermore, we show limits only for an integrated luminosity of 300 fb^{-1}. The results of Table VI demonstrate that a linear collider, with the exception of F_{1V}^{γ} and F_{2V}^{γ}, will be able to considerably improve the sensitivity limits which can be achieved at the LHC, in particular, for the ttZ couplings. For the SLHC, with 3000 fb^{-1}, we obtain bounds for the anomalous ttV couplings which are a factor $2-3$ more stringent than those shown in Table VI. Thus, even if the SLHC operates first, a linear collider will still be able to improve the ttZ anomalous coupling limits by at least a factor 3. It should be noted, however, that this picture could change once correlations between different nonstandard ttV couplings are taken into account. Unfortunately, so far, no realistic studies for $e^+e^- \to t\bar{t}$ which include these correlations have been performed. We found that there are significant correlations between the various ttV couplings at the LHC. Since both $tt\gamma$ and ttZ contribute to $e^+e^- \to t\bar{t}$, the correlations may even be larger at a e^+e^- linear collider. More detailed studies are needed in order to answer this question.

Our calculation of sensitivity bounds is subject to several uncertainties. The cross sections of the main backgrounds, $t\bar{t}j$ and $Zb\bar{b}+4j$ production, are proportional to α_s^3 and α_s^6, respectively, whereas the signal cross section scales as α_s^2. The background thus depends more strongly on the factorization and renormalization scale than the signal. The background normalization can be fixed by relaxing the $t\bar{t}\gamma$ (Eqs. (23)–(28)) or $t\bar{t}Z$ selection cuts (Eqs. (23), (26), and (32)–(34)), measuring the cross section in that background-dominated region of phase space, and then extrapolating back to the analysis region. Since $t\bar{t}j$ production is the dominant source of background in the $t\bar{t}\gamma$ case, S:B sensitively depends on the jet photon misidentification probability, $P_{j\to\gamma}$. This has been measured at the Tevatron, at least for small values of the photon transverse momentum. For the LHC, we have relied on ATLAS and CMS simulations. Finally, in calculating limits we have ignored the background from $W\gamma$ + jets and WZ+ jets production, where two of the jets are misidentified as b-quarks. While these backgrounds should be very small at the Tevatron and LHC, they may be more important at the SLHC. Fortunately, the total background for both $t\bar{t}\gamma$ and $t\bar{t}Z$ production is relatively small and hardly affects the ultimate sensitivity limits. Increasing the background cross section by a factor 2, for example, weakens the bounds by only a few percent.

In our analysis, we have assumed that both b quarks are tagged. If events with only one b tag can be utilized, the sensitivity bounds can be improved by up to a factor 1.5. However, detailed background calculations are needed before a firm conclusion can be drawn. The same statement applies to the $\not{p}_T b\bar{b}+4j$ final state, which has the potential of improving the sensitivity limits for anomalous ttZ couplings by as much as a factor 1.7. Finally, we stress that our calculation was based on a simple χ^2 test. More powerful statistical tools such as those used in the recent reanalysis of the top quark mass [4], or a neural net analysis, may further improve the limits.

VI. SUMMARY AND CONCLUSIONS

Currently, little is known about top quark couplings to the photon and Z boson. There are no direct measurements of these couplings; indirect measurements, using LEP data, tightly constrain only the ttZ vector and axial vector couplings. All others are only very weakly constrained by LEP and/or $b \to s\gamma$ data. The ttV ($V=\gamma, Z$) couplings can be measured directly in $e^+e^- \to t\bar{t}$ at a future e^+e^- linear collider. However, such a machine is at least a decade away. In addition, the process $e^+e^- \to t\bar{t}$ is simultaneously sensitive to $tt\gamma$ and ttZ couplings, and significant cancellations between various couplings may occur.

In this paper, we have considered $t\bar{t}\gamma$ production (including radiative top decay, $t \to Wb\gamma$, in $t\bar{t}$ events) and $t\bar{t}Z$ production at hadron colliders as tools to measure the ttV couplings. We calculated the signal cross sections, taking into account all top quark-resonant Feynman diagrams. In $t\bar{t}\gamma$ production, we concentrated on the $\gamma\ell\nu b\bar{b}jj$ final state. For $t\bar{t}Z$ production, we assumed that the Z boson decays leptonically, $Z \to \ell'^+\ell'^-$, and investigated the $\ell'^+\ell'^-\ell\nu b\bar{b}jj$ (trilepton) and $\ell'^+\ell'^- b\bar{b}+4j$ (dilepton) final states. All relevant background processes were included. Once $t\bar{t}\gamma$ or $t\bar{t}Z$ selection cuts are imposed, the total background is substantially smaller than the signal. The dominant background source for $t\bar{t}\gamma$ events is QCD $t\bar{t}j$ production, where one jet is misidentified as a photon. For $t\bar{t}Z$ production, $Zb\bar{b}+4j$ production and singly-resonant processes are the main sources. In all our calculations we assumed that both b quarks are tagged.

At the Tevatron, the $t\bar{t}Z$ cross section is too small to be observable. The $t\bar{t}\gamma$ cross section is large enough to allow for a first, albeit not very precise, test of the $tt\gamma$ vector and axial vector couplings, provided that an integrated luminosity of more than 5 fb^{-1} can be accumulated. No useful limits on the dipole form factors $F_{2V,A}^{\gamma}$ can be obtained. Since $q\bar{q}$ annihilation dominates at Tevatron energies, initial state photon radiation severely limits the sensitivity of $t\bar{t}\gamma$ production to anomalous top quark couplings.

This is not the case at the LHC where gluon fusion is the dominant production mechanism. Combined with a much larger cross section, this results in much-improved sensitivity limits. Already with an integrated luminosity of 30 fb^{-1}, which is expected after the first 3 years of operation, one can probe the $tt\gamma$ couplings with a precision of about $10-35\%$ per experiment. With 300 fb^{-1}, which corresponds to 3 years of running at design luminosity, a $4-7\%$ measurement of the $tt\gamma$ vector and axial vector couplings can be expected, while the dipole form factors

$F^{\gamma}_{2V,A}$ can be measured with 20% accuracy. Finally, if the luminosity of the LHC can be upgraded by a factor of 10 (the SLHC program) without significant loss of particle detection efficiency for photons, leptons and b quarks, these limits can be improved by another factor $2-3$.

The $t\bar{t}Z$ cross section with leptonic Z decays is roughly a factor 20 smaller than the $t\bar{t}\gamma$ rate. It is therefore not surprising that the sensitivity limits on the ttZ couplings are significantly weaker than those which one expects for the $tt\gamma$ couplings. We found that, for 300 fb^{-1}, the ttZ vector (axial vector) couplings can be measured with a precision of $45-85\%$ ($15-20\%$), and $F^{Z}_{2V,A}$ with a precision of $50-55\%$. At the SLHC, these bounds can be improved by factors of $1.4-2$ (≈ 3) and 1.6, respectively.

In our analysis, we conservatively assumed that both b quarks are tagged, and used a simple χ^2 test to derive sensitivity limits. If single-b-tag events can be utilized, the sensitivity bounds can be significantly strengthened. Further improvements could also result from using more powerful statistical tools, similar to those which have been used recently to measure the top quark mass [4].

ACKNOWLEDGMENTS

We would like to thank E. Boos, R. Demina, J. Parsons, P. Tipton and D. Toback for useful discussions. One of us (U. B.) would like to thank the Fermilab Theory Group, where part of this work was carried out, for its generous hospitality. This research was supported in part by the National Science Foundation under grant No. PHY-0139953 and the Department of Energy under grant DE-FG02-91ER40685. Fermilab is operated by Universities Research Association Inc. under Contract No. DE-AC02-76CH03000 with the U. S. Department of Energy.

[1] CDF Collaboration, F. Abe *et al.*, Phys. Rev. Lett. **74**, 2626 (1995).
[2] D0 Collaboration, S. Abachi *et al.*, Phys. Rev. Lett. **74**, 2632 (1995).
[3] D. Chakraborty, J. Konigsberg, and D. L. Rainwater, Annu. Rev. Nucl. Part. Sci. **53**, 301 (2003).
[4] D0 Collaboration, V. M. Abazov *et al.*, Nature (London) **429**, 638 (2004) and references therein.
[5] R. S. Chivukula, S. B. Selipsky, and E. H. Simmons, Phys. Rev. Lett. **69**, 575 (1992); R. S. Chivukula, E. H. Simmons, and J. Terning, Phys. Lett. B **331**, 383 (1994); K. Hagiwara and N. Kitazawa, Phys. Rev. D **52**, 5374 (1995); U. Mahanta, Phys. Rev. D **55**, 5848 (1997); Phys. Rev. D **56**, 402 (1997).
[6] F. Larios, M. A. Perez, and C. P. Yuan, Phys. Lett. B **457**, 334 (1999); M. Frigeni and R. Rattazzi, Phys. Lett. B **269**, 412 (1991).
[7] R. D. Peccei, S. Peris, and X. Zhang, Nucl. Phys. B **349**, 305 (1991); G. L. Kane, G. A. Ladinsky, and C. P. Yuan, Phys. Rev. D **45**, 124 (1992); M. Jezabek and J. H. Kuhn, Phys. Lett. B **329**, 317 (1994); C. A. Nelson, B. T. Kress, M. Lopes, and T. P. McCauley, Phys. Rev. D **56**, 5928 (1997); C. A. Nelson, B. T. Kress, M. Lopes, and T. P. McCauley, Phys. Rev. D **57**, 5923 (1998).
[8] R. H. Dalitz and G. R. Goldstein, Proc. R. Soc. London A **455**, 2803 (1999).
[9] CDF Collaboration, T. Affolder *et al.*, Phys. Rev. Lett. **86**, 3233 (2001).
[10] F. del Aguila and J. A. Aguilar-Saavedra, Phys. Rev. D **67**, 014009 (2003).
[11] S. Cortese and R. Petronzio, Phys. Lett. B **253**, 494 (1991).
[12] S. S. D. Willenbrock and D. A. Dicus, Phys. Rev. D **34**, 155 (1986).
[13] A. P. Heinson, A. S. Belyaev, and E. E. Boos, Phys. Rev. D **56**, 3114 (1997).
[14] E. Boos, L. Dudko, and T. Ohl, Eur. Phys. J. C **11**, 473 (1999).
[15] E. Boos, A. Pukhov, M. Sachwitz, and H. J. Schreiber, Phys. Lett. B **404**, 119 (1997); J. J. Cao *et al.*, Phys. Rev. D **58**, 094004 (1998).
[16] E. Boos, M. Dubinin, M. Sachwitz, and H. J. Schreiber, Eur. Phys. J. C **16**, 269 (2000).
[17] B. Grzadkowski and Z. Hioki, Phys. Rev. D **61**, 014013 (2000).
[18] B. Grzadkowski and Z. Hioki, Nucl. Phys. **B585**, 3 (2000).
[19] Z. H. Lin *et al.*, Phys. Rev. D **65**, 014008 (2002).
[20] American Linear Collider Working Group Collaboration, T. Abe *et al.*, hep-ex/0106057.
[21] ECFA/DESY LC Physics Working Group, J. A. Aguilar-Saavedra *et al.* hep-ph/0106315.
[22] R. Frey, hep-ph/9606201.
[23] G. A. Ladinsky and C. P. Yuan, Phys. Rev. D **49**, 4415 (1994).
[24] H. Y. Zhou, hep-ph/9806323.
[25] U. Baur, M. Buice, and L. H. Orr, Phys. Rev. D **64**, 094019 (2001).
[26] S. Y. Choi and K. Hagiwara, Phys. Lett. B **359**, 369 (1995); M. S. Baek, S. Y. Choi, and C. S. Kim, Phys. Rev. D **56**, 6835 (1997); P. Poulose and S. D. Rindani, Phys. Rev. D **57**, 5444 (1998); [**61**, 119902(E) (2000)]; Phys. Lett. B **452**, 347 (1999).
[27] A. Djouadi, J. Ng, and T. G. Rizzo, hep-ph/9504210.
[28] W. Hollik *et al.*, Nucl. Phys. **B551**, 3 (1999); [**B557**, 407(E) (1999)].
[29] W. F. L. Hollik, Fortschr. Phys. **38**, 165 (1990).
[30] J. Bernabeu, D. Comelli, L. Lavoura, and J. P. Silva, Phys. Rev. D **53**, 5222 (1996).
[31] J. M. Cornwall, D. N. Levin, and G. Tiktopoulos, Phys. Rev. Lett. **30**, 1268 (1973); Phys. Rev. D **10**, 1145 (1974); C. H. Llewellyn Smith, Phys. Lett. B **46**, 233 (1973); S. D.

Joglekar, Ann. Phys. (N.Y.) **83**, 427 (1974).
[32] M. Hosch, K. Whisnant, and B. L. Young, Phys. Rev. D **55**, 3137 (1997).
[33] G. Altarelli, R. Barbieri, and S. Jadach, Nucl. Phys. **B369**, 3 (1992); [**B376**, 444(E) (1992)]; G. Altarelli, R. Barbieri, and F. Caravaglios, Nucl. Phys. **B405**, 3 (1993).
[34] G. Altarelli, hep-ph/0406270.
[35] G. Altarelli, R. Barbieri, and F. Caravaglios, Int. J. Mod. Phys. A **13**, 1031 (1998).
[36] O. J. P. Eboli, M. C. Gonzalez-Garcia, and S. F. Novaes, Phys. Lett. B **415**, 75 (1997).
[37] J. L. Hewett and T. G. Rizzo, Phys. Rev. D **49**, 319 (1994).
[38] Particle Data Group Collaboration, S. Eidelman *et al.*, Phys. Lett. B **592**, 1 (2004).
[39] M. Neubert, hep-ph/0408179.
[40] U. Baur, J. A. M. Vermaseren, and D. Zeppenfeld, Nucl. Phys. **B375**, 3 (1992).
[41] F. Maltoni, D. L. Rainwater, and S. Willenbrock, Phys. Rev. D **66**, 034022 (2002).
[42] J. Pumplin *et al.*, J. High Energy Phys. 07 (2002) 012.
[43] CDF Collaboration, F. Abe *et al.*, Report No.FERMILAB-Pub-96/390-E, 1996 (unpublished).
[44] CMS Collaboration, M. Della Negra *et al.*, CMS Letter of Intent, CERN-LHCC-92-3, 1992 (unpublished); CMS Collaboration, G. L. Bayatian *et al.*, CMS Technical Design Report No. CERN-LHCC-94-38, 1994 (unpublished).
[45] F. Maltoni and T. Stelzer, J. High Energy Phys. 02 (2003) 027.
[46] CDF Collaboration, D. Acosta *et al.*, hep-ex/0410041.
[47] F. Gianotti *et al.*, Eur. Phys. J. C **39**, 293 (2005).
[48] CDF Collaboration, D. Acosta *et al.*, Phys. Rev. Lett. (to be published).
[49] D0 Collaboration, V. M. Abazov *et al.*, DØ public note 4488.
[50] ATLAS TDR, Report No. CERN/LHCC/99-15, 1999 (unpublished).
[51] Ph. Schwemling, ATLAS note SN-ATLAS-2003-034.
[52] S. Abdullin *et al.*, Phys. Lett. B **431**, 410 (1998).
[53] V. D. Barger, K. M. Cheung, T. Han, and R. J. Phillips, Phys. Rev. D **42**, 3052 (1990).
[54] B. Grzadkowski, B. Lampe, and K. J. Abraham, Phys. Lett. B **415**, 193 (1997).
[55] G. Mahlon and S. J. Parke, Phys. Lett. B **347**, 394 (1995).
[56] G. Altarelli, L. Conti, and V. Lubicz, Phys. Lett. B **502**, 125 (2001); R. Decker, M. Nowakowski, and A. Pilaftsis, Z. Phys. C **57**, 339 (1993); E. Jenkins, Phys. Rev. D **56**, 458 (1997).
[57] M. L. Mangano *et al.*, J. High Energy Phys. 07 (2003) 001.
[58] M. Beneke *et al.*, hep-ph/0003033 and references therein.
[59] U. Baur and E. L. Berger, Phys. Rev. D **47**, 4889 (1993).